Geochemical signature of the Egersund basaltic dyke swarm, SW Norway, in the context of late-Neoproterozoic opening of the Iapetus Ocean

BERNARD BINGEN & DANIEL DEMAIFFE

Bingen, B. & Demaiffe, D.: Geochemical signature of the Egersund basaltic dyke swarm, SW Norway, in the context of late-Neoproterozoic opening of the Iapetus Ocean. *Norsk Geologisk Tidsskrift,* Vol. 79, pp. 69–86. Oslo 1999. ISSN 0029-196X.

The Egersund basaltic dyke swarm is made up of 11 ESE–WNW-trending dykes in the Proterozoic crystalline basement of southwest Norway. Two types of dyke occur: porphyritic dykes with plagioclase phenocrysts and aphyric dykes. Limited magmatic differentiation occurred in the dykes during shallow level intrusion. The porphyritic dykes and one of the aphyric dykes have subalkaline to mildly alkaline compositions, whereas the other aphyric dykes have alkaline compositions. The most primitive magmas occur in the porphyritic dykes; they have Mg numbers of 56–61, TiO_2 contents of 2.0–2.1% and enriched incompatible trace element contents. Initial isotopic compositions, Sr_i and $\varepsilon(Nd)_i$, are 0.7034–0.7039 and +2.0–+3.1 respectively. The most evolved magmas in alkaline dykes are SiO_2-poor (45–46%) ferrobasalts, very enriched in TiO_2 (3.2–3.4%), P_2O_5 (2.0–2.5%) and incompatible trace elements. They have Sr_i of 0.7058–0.7060 and $\varepsilon(Nd)_i$ of +1.0. The compositions of the most primitive magmas and minerals suggest that the porphyritic dykes tapped a magma chamber situated at the crust–mantle boundary, at ca. 10 kbar. It is shown that one of the aphyric dykes is possibly related to the porphyritic dyke magma by a fractional crystallization process accompanied by limited crustal assimilation at this pressure. The alkaline dykes represent a distinct suite with a distinct mantle source. The 616 ± 3 Ma Egersund Swarm is placed in the geotectonic context of late-Neoproterozoic rifting leading to opening of the Iapetus Ocean. At the Baltoscandian passive margin of Baltica, there is a first order 'oceanwards' decrease in incompatible trace element contents and Sr_i and an increase of $\varepsilon(Nd)_i$ values of basaltic dyke swarms, from the Egersund Swarm in the continental basement, to the sheeted dyke complexes situated at the continent–ocean transition. This geochemical trend is interpreted as a change from high-pressure partial melting of garnet peridotite with residual garnet in a mildly depleted mantle, to lower-pressure partial melting of a depleted mantle.

B. Bingen, Geological Survey of Norway, 7491 Trondheim, Norway (bernard.bingen@ngu.no); D. Demaiffe, Département des Sciences de la Terre et de l'Environnement, CP160/02, Université Libre de Bruxelles, 1050 Bruxelles, Belgium (ddemaif@ulb.ac.be).

Introduction

Proterozoic continental passive margins are generally deeply eroded or strongly reworked in younger orogens so that the record of ancient rifting events is fragmentary. Major rifting events and opening of oceanic basins are commonly associated with large volumes of basaltic magmatism (e.g. Saunders et al. 1997). Dyke swarms represent direct evidence for magma generation and intrusion in extensional stress regimes, and possibly correspond to the subsurface expression of an eroded magmatic province of significant volume (Ernst & Buchan 1997). In this context, geochronological and geochemical studies of dyke swarms can help unravel the history of specific Proterozoic rifting events.

Following the Grenvillian/Sveconorwegian orogeny (1.25–0.90 Ga), Baltica (Scandinavia + Russia + Ukraine) entered a period of extensional tectonic regime. Intracratonic sedimentary basins formed during the Neoproterozoic in rifts and aulacogens (Kumpulainen & Nystuen 1985; Vidal & Moczydlowska 1995). During the late-Neoproterozoic, one of these basins evolved into an ocean, the Iapetus Ocean, which opened between Baltica, Siberia, Laurentia (North America + Greenland + Scotland), Amazonia and the craton of Rio de la Plata (see reviews of Roberts & Gale 1978; Torsvik et al. 1996; Dalziel 1997). Later in the Paleozoic, closure of Iapetus occurred during the Caledonian orogeny (summary of plate movements in Torsvik 1998). Geologic formations of the northwestern (present-day orientation) Baltica–Iapetus passive margin, also called the Baltoscandian margin, include thick sedimentary sequences intruded by basaltic dyke swarms (Andréasson 1994; Andréasson et al. 1998). This margin is now exposed in allochthons of the Caledonian Orogen, called the Seve–Kalak Superterrane. In the Sveconorwegian crystalline basement of south Norway, evidence for late-Neoproterozoic rifting is scarce, but includes the intrusion of the Egersund dyke swarm (Antun 1955; Venhuis & Barton 1986; Sundvoll 1987; Miller et al. 1996). Recent dating of this swarm at 616 ± 3 Ma (baddeleyite U-Pb age; Bingen et al. 1998b) shows that it is almost coeval with swarms situated in the Caledonian allochthons (608 ± 1 Ma; Svenningsen 1994, 1996), so that together, these different magmatic suites form a late-Neoproterozoic magmatic province of significant volume and geographical extent.

In this paper new petrological, geochemical and isotopic (Sr and Nd) data are presented on the Egersund Swarm. The objectives are to characterize this magmatic event, to assess the relationships between the different dykes

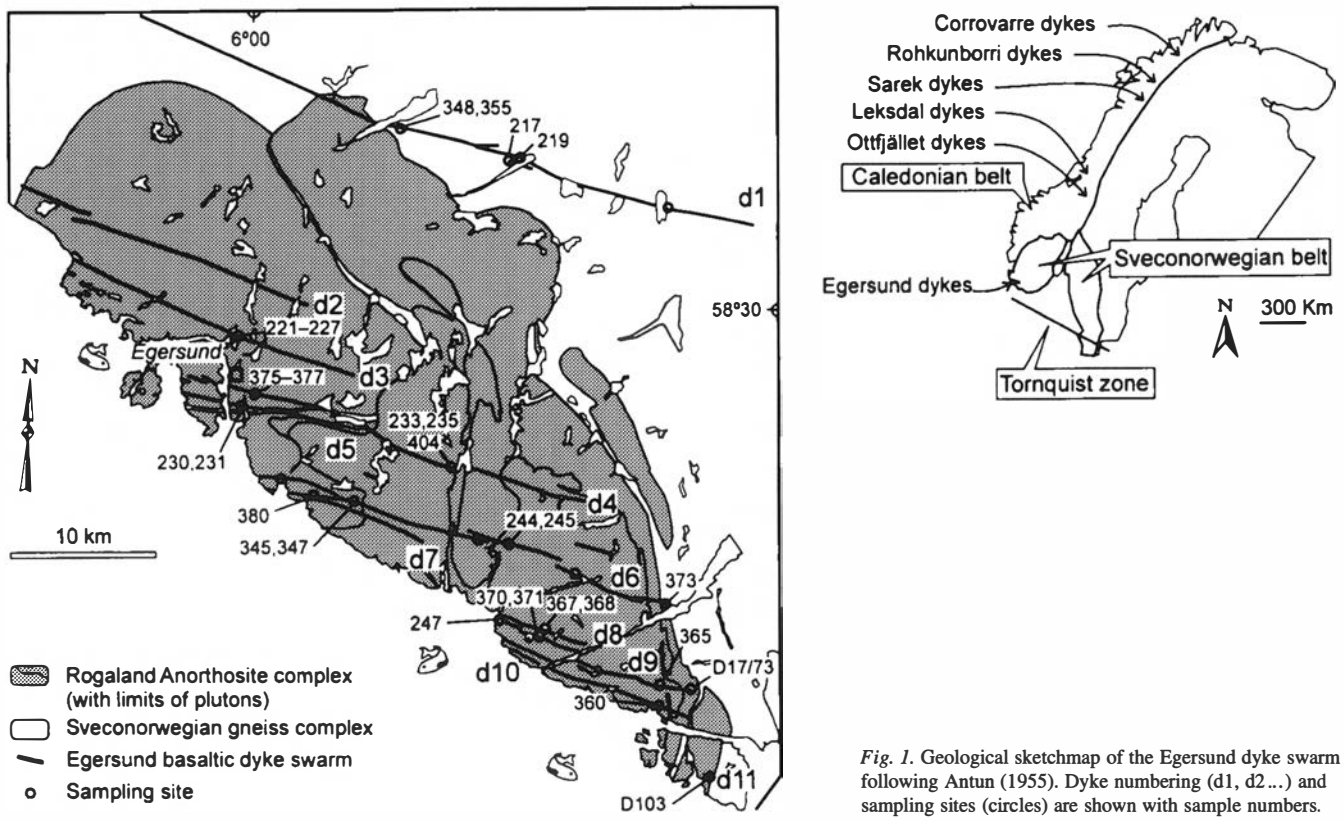

Fig. 1. Geological sketchmap of the Egersund dyke swarm following Antun (1955). Dyke numbering (d1, d2...) and sampling sites (circles) are shown with sample numbers.

(crystallization processes and continental lithospheric contamination) and to compare the Egersund Swarm with other swarms of the Baltoscandian margin in order to picture the magmatic activity associated with Iapetus opening.

Geological setting of the Egersund Swarm

In south-westernmost Norway, the Sveconorwegian province is made up of a high-grade Proterozoic gneiss terrane (Bingen & van Breemen 1998). It is intruded by voluminous 0.98–0.92 Ga post-tectonic plutonic complexes, including the 0.93 Ga Rogaland anorthosite complex (Pasteels et al. 1979; Schärer et al. 1996). Post-orogenic Sveconorwegian regional cooling/unroofing is constrained by hornblende $^{40}Ar/^{39}Ar$ ages ranging from 0.93 to 0.85 Ga, and by Rb-Sr biotite–whole-rock ages ranging from 0.90 to 0.85 Ga (data and compilation in Verschure et al. 1980; Bingen et al. 1998a). The high-grade terrane is intruded by two basaltic dyke swarms, the WSW–ENE-trending Hunnedalen swarm dated at 855 ± 59, 835 ± 47 Ma (Sm-Nd internal isochron ages) or 848 ± 27 Ma ($^{40}Ar/^{39}Ar$ biotite plateau age) (Maijer & Verschure 1998; Walderhaug et al. in press) and the WNW–ESE-trending Egersund Swarm.

The Egersund Swarm consists of 11 subvertical dykes numbered d1 to d11 from north to south by Antun (1955, Fig. 1). The largest dyke (d1) is 60 km long and 30 m wide at maximum. The smallest dyke (d11) is a few km long and ca. 50 cm wide. The dykes are not affected by deformation. They are almost parallel and do not crosscut each other, suggesting that they are related to a single magmatic event. Detailed mapping in the southern part of the Rogaland anorthosite complex (Karlsen et al. 1998) shows that the dykes are discontinuous and locally divided into several sub-dykes. Contacts between the dykes and their wallrocks are sharp (<5 mm). Fine-grained to glassy chilled margins a couple of centimetres wide are observed. Glass is locally a major constituent in chilled margins of thin sub-dykes of dykes 1, 4 and 5 (Antun 1955), testifying to a fast cooling rate. Grain size increases progressively up to approximately 1 mm towards the centre of large dykes. Crustal xenoliths were observed in dykes 1 and 6, where they are locally abundant (Antun 1955; Venhuis & Barton 1986).

The 616 ± 3 Ma age of the Egersund Swarm and its setting indicates that it is not linked to Sveconorwegian post-orogenic relaxation, but represents a younger and independent late-Neoproterozoic subvolcanic magmatic event. The direction of the swarm points to a component of crustal extension perpendicular to the ESE–WNW trend. This direction is parallel to the south-western Tornquist margin of Baltica (Fig. 1), suggesting that the intrusion of the swarm is related to a phase of rifting, which eventually led to the opening of the Iapetus Ocean and its Tornquist arm.

Analytical methods

Samples were collected in traverses across dykes 1, 3, 4–6 and 8–11. Only the freshest samples with well-preserved

Table 1. Analyses of representative samples of the Egersund Swarm.

Sample	B219	B348	B224	B233	B235	B376	B231	B245	B345	B247	B367	B365	B360	D103
dyke [a]	d1(c)	d1(c)	d3(c)	d4(m)	d4(c)	d4(c)	d5(c)	d6(c)	d6(c)	d8(c)	d8(c)	d9(c)	d10(c)	d11(c)
SiO_2 (wt%)	46.5	47.6	46.8	45.8	46.2	46.3	44.8	50.4	50.7	46.2	47.3	46.3	45.8	45.8
TiO_2	2.78	3.00	1.99	3.45	3.20	3.19	3.24	2.10	2.06	2.13	2.44	1.72	2.01	1.76
Al_2O_3	15.7	15.5	16.0	14.3	14.4	14.35	13.8	15.4	15.7	16.5	15.06	17.32	16.73	16.56
Fe_2O_3	4.52	3.82	3.02	3.96	3.53	3.47	3.53	3.18	2.50	3.07	2.97	2.79	3.61	2.55
FeO	7.96	9.09	7.15	10.39	10.71	10.88	10.39	8.12	8.67	7.90	9.03	7.10	7.26	6.90
MnO	0.18	0.20	0.16	0.22	0.22	0.22	0.21	0.17	0.17	0.16	0.17	0.15	0.15	0.15
MgO	5.67	5.93	8.60	4.98	4.82	4.80	4.89	6.16	6.27	7.68	6.28	8.09	8.09	7.49
CaO	8.59	7.64	11.00	7.52	7.26	7.23	7.36	8.77	8.67	10.09	9.03	10.79	10.22	10.55
Na_2O	3.05	3.55	2.16	3.70	3.97	3.89	3.52	3.13	3.18	2.61	2.89	2.44	2.28	2.48
K_2O	1.63	1.77	0.27	2.44	2.68	2.69	2.22	1.43	1.41	0.23	0.06	0.30	0.25	0.12
P_2O_5	0.67	0.76	0.29	2.42	2.50	2.47	2.34	0.31	0.34	0.26	0.36	0.25	0.27	0.30
LOI	3.69	1.88	3.56	1.82	1.17	1.27	4.14	1.60	1.28	4.38	4.01	3.06	3.41	5.70
Sum	100.9	100.7	100.9	101.0	100.6	100.8	100.4	100.8	100.9	101.1	99.6	100.3	100.1	100.4
Sc (ppm)	19.4	20.4	26.2	16.4	16.0	15.8	16.2	25.9	25.6	24.1	25.9	24.4	23.6	23.4
Cr	23	18	129	<5	<6	<5	<6	28	26	30	11	44	29	103
Co	50.9	50.9	49.1	10.9	41.2	40.1	42.3	44.2	44.6	53.0	52.0	49.3	54.6	45.1
Ni	64	55	86	16	13	15	16	52	52	65	41	72	75	86
Ba	638	807	137	1686	1904	1894	1665	393	405	150	297	172	196	233
Rb	83	38	2	40	41	40	36	27	26	10	20	6	2	16
Sr	608	628	428	589	632	620	593	394	391	437	399	447	440	425
Y	32	35	23	60	61	61	58	31	32	24	31	21	23	22
Zr	194	217	148	295	296	297	287	232	228	158	205	126	148	141
Hf	4.4	5.1	3.41	7.0	7.0	6.7	6.6	5.3	5.3	3.6	5.0	2.90	3.49	3.28
Nb	31	35	17	45	46	47	42	24	24	18	23	16	19	18
Ta	2.5	2.9	1.48	3.5	3.6	3.6	3.3	1.87	2.01	1.45	1.76	1.18	1.37	1.49
La	32.8	36.9	15.3	64.6	66.7	65.4	61.7	27.0	27.1	15.6	21.7	13.1	15.0	15.9
Ce	70	83	36.2	151	151	149	143	59.9	61.1	37.4	53.6	31.3	36.1	36.8
Nd	36.5	43.5	21.3	86	87	84	82	30.9	33.1	22.1	30.1	18.9	20.9	21.2
Sm	8.0	9.0	5.01	17.5	17.4	17.1	16.6	6.8	6.9	5.27	6.9	4.41	5.11	4.91
Eu	2.58	2.91	1.77	6.59	6.78	6.61	6.28	2.14	2.17	1.80	2.16	1.57	1.75	1.72
Tb	1.04	1.18	0.73	2.24	2.19	2.12	2.09	0.98	1.02	0.77	1.01	0.66	0.75	0.69
Yb	2.27	2.68	1.77	4.3	4.1	4.0	3.9	2.69	2.68	1.79	2.41	1.58	1.70	1.66
Lu	0.33	0.37	0.24	0.55	0.57	0.56	0.54	0.38	0.38	0.25	0.34	0.21	0.25	0.24
Th	2.6	3.2	1.33	4.1	4.2	4.0	3.8	2.5	2.5	1.40	2.32	1.15	1.30	1.35
U	0.75	1.07	0.32	1.00	1.02	1.00	0.88	0.67	0.76	0.29	0.55	0.23	0.37	0.28

[a] (c): centre of the dyke; (m): <30 cm margin.

magmatic mineral associations were selected for analysis. Electron microprobe analyses of minerals were obtained for 8 samples at 15 kV accelerating voltage (CAMST; UCL Louvain; Appendixes 1–5). Fifty-six whole-rock samples collected in the centres and margins of the dykes were analysed by XRF on pressed powder pellets for Ti, K, P, Ni, Rb, Sr, Y, Zr and Nb; a calibration based on regression of several international standards and Mo Kα-Compton peak for matrix correction was used (ULB Bruxelles; Appendix 6). Thirty samples were selected for complete major element analyses (XRF on fused glass disks for Si, Al, Fe, atomic absorption for Mn, Mg, Ca, Na, K and permanganate titration for Fe^{2+}; MRAC Tervuren; Appendix 7). A subset of 14 samples was analysed for trace elements by INAA (Table 1; KUL Leuven; method and precision in Pedersen & Hertogen 1990).

Sr isotopic data were acquired for 21 whole-rock samples and Nd isotopic data for 7 of them (Tables 2, 3; ULB Bruxelles; method described in Weis et al. 1987). Sr isotopic composition was measured with a single collector Finnigan Mat 260 mass spectrometer, whereas Nd isotopic composition was measured with a multicollector VG Sector 54 spectrometer.

Summary of petrologic data

Petrography

In the Egersund Swarm, two groups of dykes are defined on the basis of their texture: porphyritic (d3, d7–d11) and aphyric (d1–d2, d4–d6). Porphyritic dykes display zoned, up to 1 cm long, phenocrysts of bytownite (An81 to An73 in the core). The matrix typically has a subophitic texture with plagioclase laths (An73 to An53), augite and olivine (Fo82.5 to Fo63) and minor titano-magnetite and hemo-ilmenite. Olivine crystals are locally larger than augite. Interstitial brown biotite, quartz and K-feldspar are common. Large plagioclase phenocrysts are found in the centre of the thinnest dykes, and phenocrysts are locally deformed; these observations suggest that crystallization of phenocrysts started prior to intrusion at shallow level (Antun 1955; Venhuis & Barton 1986). The aphyric dykes show a subophitic texture; they have plagioclase (An61 to An40), augite and minor titano-magnetite and hemo-ilmenite. In dykes 1 and 6, olivine is common but not ubiquitous, and in dykes 4 and 5, Fe-rich olivine (Fo47) is abundant. Interstitial biotite, apatite, quartz and K-feldspar

Table 2. Whole-rock Sr isotopic data.

Sample	Dyke	Rb[a] (ppm)	Sr[a] (ppm)	$^{87}Rb/^{86}Sr$	$^{87}Sr/^{86}Sr$	$\pm 2\sigma$[b]
B219	d1(c)	83	608	0.3958	0.70803	4
B348	d1(c)	38	628	0.1728	0.70614	4
B355	d1(c)	36	596	0.1743	0.70615	9
B221	d3(m)	2.0	401	0.0141	0.70399	2
B224	d3(c)	2.3	428	0.0155	0.70357	5
B233	d4(m)	40	589	0.1963	0.70749	9
B235	d4(c)	41	632	0.1857	0.70762	4
B375	d4(m)	40	622	0.1853	0.70747	3
B376	d4(c)	40	620	0.1875	0.70755	3
B231	d5(c)	36	593	0.1775	0.70734	6
B245	d6(c)	27	394	0.1977	0.70716	4
B345	d6(c)	26	391	0.1952	0.70715	6
B373	d6(c)	28	380	0.2152	0.70807	3
B380	d6(c)	2.4	366	0.0186	0.70568	6
B247	d8(c)	10	437	0.0672	0.70442	3
B367	d8(c)	20	399	0.1427	0.70601	4
B368	d8(c)	21	398	0.1492	0.70589	5
B365	d9(c)	6.1	447	0.0395	0.70414	3
D1773	d9(c)	15	402	0.1085	0.70444	3
B360	d10(c)	1.7	440	0.0108	0.70393	4
D103	d11(c)	16	425	0.1093	0.70486	3

[a] XRF on powder pellets.
[b] Error on last digit.

Table 3. Whole-rock Nd isotopic data.

Sample	Dyke	Nd[a] (ppm)	Sm[a] (ppm)	$^{147}Sm/^{144}Nd$	$^{143}Nd/^{144}Nd$	$\pm 2\sigma$[b]
B219	d1(c)	36.5	8.0	0.1325	0.512410	7
B224	d3(c)	21.3	5.01	0.1422	0.512534	8
B235	d4(c)	87	17.4	0.1209	0.512384	7
B245	d6(c)	30.9	6.8	0.1330	0.512448	8
B365	d9(c)	18.9	4.41	0.1411	0.512572	7
B360	d10(c)	20.9	5.11	0.1478	0.512586	16
D103	d11(c)	21.2	4.91	0.1400	0.512510	7

[a] INAA.
[b] Error on last digits.

are present. Acicular apatite is especially abundant in dykes 4 and 5.

Most dykes are variably affected by hydrothermal alteration. Plagioclase is commonly altered to sericite; olivine and ilmenite are commonly retrogressed. Minerals attributed to alteration include carbonates, quartz, chlorite, epidote, prehnite, actinolite and leucoxene (Venhuis & Barton 1986). The common occurrence of carbonate and carbonate-bearing spherical aggregates indicates that alteration of the dykes was accomplished by CO_2-bearing fluids, and suggests that the initial magmatic fluids were CO_2-rich (Antun 1955; Venhuis & Barton 1986).

Geothermometry

Two-oxide geothermometry was applied to 6 samples using the QUILF calibration of Lindsley & Frost (1992). Oxide pairs of all samples but one plot close to the QFM oxygen buffer (less than $\pm$ 0.8 log units from QFM, Fig. 2a). In sample B224 (d3), where some alteration of oxides and olivine is observed in thin section, calculated pO_2 is higher (1.4–2.7 log units above QFM). Calculated temperatures range from 1020 to 710°C; the highest temperatures are recorded in the thinnest dyke 11 (sample D103: 1020–940°C). These values are probably close to magmatic crystallization temperatures. In the other samples, oxides have been largely re-equilibrated during subsolidus cooling.

Fe-Mg exchange geothermometry between olivine and augite using the calibration of Loucks (1996) yields temperatures of 1250–1180°C in porphyritic dyke 11 (sample D103), 1150–1145°C in porphyritic dyke 8 (sample B367, 2 m from contact) and 1055–986°C in aphyric dyke 4 (sample B235, 8 m from contact) (Fig. 2b). In dykes 8 and 11, these temperatures are characteristic of magmatic crystallization, whereas in dyke 4, subsolidus Fe-Mg exchange probably took place.

Geochemical signature of the Egersund Swarm

Major and trace element signatures

In the porphyritic dykes, most samples, including those from the margins of the dykes, contain phenocrysts. At two sampling sites, dykes 3 and 8 occur as two or three sub-dykes poor in phenocrysts. Two samples (B224, B247, Table 1) collected in the centre of 2-m wide sub-dykes are almost free of phenocrysts, and their composition thus probably approaches that of the magma at the time of intrusion. They have Mg numbers [Mg# = 100 × Mg /

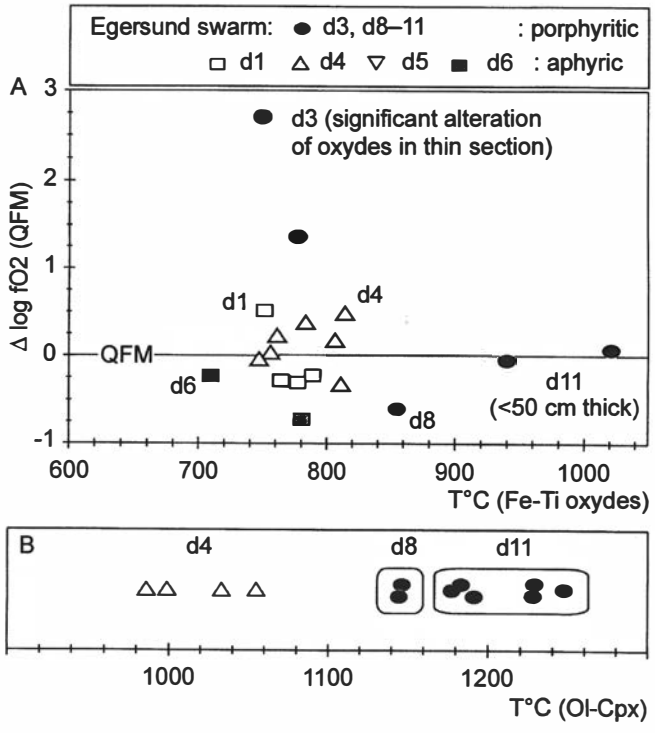

Fig. 2. (A) Temperature–fO_2 calculated for Fe-Ti oxides in six samples. Calculations were performed with the QUILF program of Lindsley & Frost (1992); the Mg-bearing equilibria are not included in the calculation owing to probable low-temperature reset. (B) Fe-Mg exchange geothermometry between olivine and augite using the calibration of Loucks (1996).

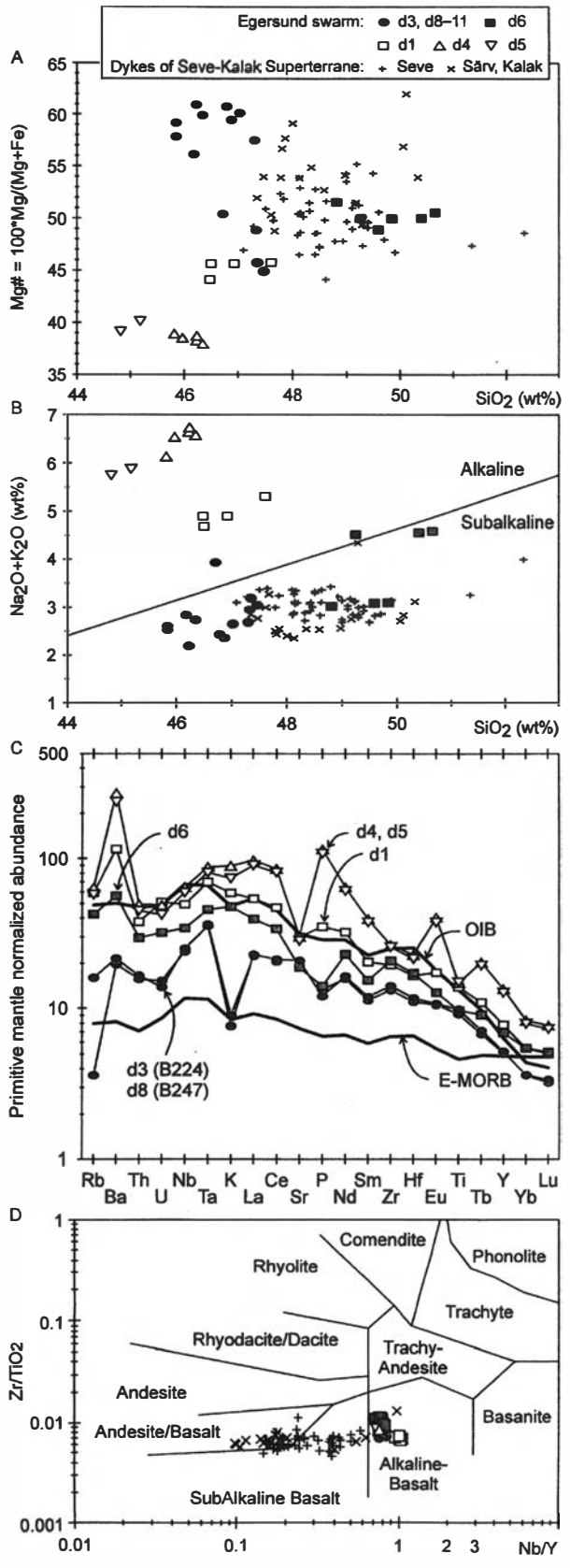

Fig. 3. Whole-rock geochemical signatures of the Egersund Swarm. Comparison with other swarms of the Baltoscandian margin now situated in the Caledonian Särv, Kalak and Seve Nappe complexes (references in text). (A) Mg# – SiO_2 diagram. (B) $Na_2O + K_2O - SiO_2$ diagram. (C) Primitive mantle normalized multi-element diagrams. Typical patterns for E-type MORB and OIB are displayed. Reference patterns and normalization values following Sun & McDonough (1989). (D) Zr/TiO_2 – Nb/Y classification diagram.

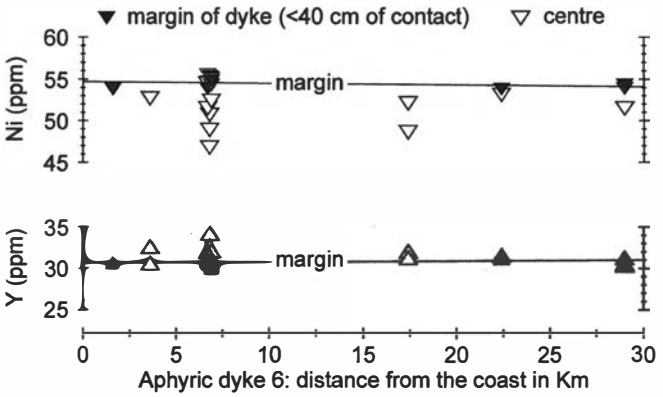

Fig. 4. Ni and Y contents (ppm) for six traverses in dyke 6 sampled over a distance of approximately 30 km. The Ni and Y contents are invariable in the margin of the dykes at the different sampling sites: Ni = 54.5 ± 1.2 ppm ($n = 10, \pm 2\sigma$), Y = 30.8 ± 0.8 ppm. Some variation is observed towards the centre of the dyke; the largest spread in composition is observed along the third traverse ($n = 13$) where dyke 6 consists of 3 parallel sub-dykes. There, Ni decreases by 8 ppm and Y increases by 4 ppm in the centre of the largest sub-dyke.

(Mg + Fe)] of 61 and 56, TiO_2 contents of 1.99 and 2.13%, and SiO_2 contents of 46.8 and 46.2% (Fig. 3a), respectively. In the binary $Na_2O + K_2O - SiO_2$ diagram, they plot in the field of subalkaline basalt (Fig. 3b). They are enriched in incompatible elements, with enrichment factors intermediate between typical values for E-MORB and OIB. Their primitive mantle normalized multi-element patterns display negative anomalies for K and Rb, and a smooth decrease in abundance for the less incompatible elements (Fig. 3c). As K and Rb are commonly mobile during hydrothermal alteration, it is not clear whether these anomalies are primary magmatic features. In the binary Zr/TiO_2–Nb/Y classification diagram of Winchester & Floyd (1977; Fig. 3d), they plot in the field of alkaline basalt, and in the ternary Th–Ta–Hf discrimination diagram of Wood (1980; not shown), in the field of alkaline within-plate basalt.

The aphyric dykes are internally more homogeneous in composition than the porphyritic dykes. Longitudinal and transversal intra-dyke variations were tested in dyke 6. The whole-rock trace element contents (e.g. Ni and Y) are constant in the margin of this dyke at six different sampling sites (Fig. 4), suggesting that intrusion of magma was fast enough that along-strike differentiation did not occur. Significant decreases of compatible elements (Ni) and increases of incompatible elements (Y) are observed towards the centre of the dyke. These trends indicate either that *in situ* crystallization, presumably starting from the walls, led to some concentration of residual magma towards the centre of the dyke, or that the fracture was filled with more evolved magma during progressive opening. Samples of chilled margins probably represent the best estimates for parent magmas of the aphyric dykes.

The different aphyric dykes display variable Mg#, SiO_2, TiO_2 and P_2O_5 contents (Fig. 3). For dyke 6, which is the richest in SiO_2 (48.8–50.7 wt%), data points plot in the subalkaline field and at the boundary between the subalka-

line and alkaline fields in the $Na_2O + K_2O - SiO_2$ diagram. Dykes 1, 4 and 5 are alkaline and characterized by low SiO_2 content (44.8–47.6 wt%) and low Mg# (38–46). In primitive mantle normalized multi-element diagrams, dykes 1 and 6 define smooth patterns enriched for the most incompatible elements. Enrichment factors are slightly below (d6) or overlapping (d1) typical values for OIB. Dyke 6 has a significant negative anomaly for P. Dykes 4 and 5 are the most enriched in incompatible elements, but the poorest in Ni. They display irregular normalized multi-element diagrams with positive anomalies in Ba and P and a deep negative anomaly in Sr. Enrichment factors are higher than typical values for OIB for most elements. In the Zr/TiO_2–Nb/Y diagram, aphyric dykes plot in the field of alkaline basalt (Fig. 3d); in the Th–Hf–Ta discrimination diagram, dyke 6 plots at the boundary between within-plate tholeiite and alkaline within-plate basalt, whereas dykes 1, 4 and 5 plot in the core of the field of alkaline within-plate basalt.

Isotopic composition

On a $^{87}Sr/^{86}Sr$–$^{87}Rb/^{86}Sr$ plot (Fig. 5a), data points for samples of the different dykes do not define an isochron. Limited variation of Rb/Sr ratios is observed in individual dykes, so reliable age calculation is impossible. However, a cluster of data points for dyke 1, dyke 6 and porphyritic dykes (except two points) displays average slopes parallel, within experimental uncertainty, to the 616 Ma reference line given by baddeleyite U-Pb dating. This suggests that the Rb-Sr isotopic system was not affected in a systematic way during post-intrusion disturbances.

Initial Sr isotopic ratios calculated at 616 Ma (Sr_i) range from 0.7034 to 0.7062 (Fig 5a). Distinct groups can be defined. Porphyritic dykes have the lowest Sr_i; all samples but two (B367, B368), cluster between 0.7034 and 0.7039, with an average value of 0.7037 ± 0.0004. Aphyric dykes have significantly more radiogenic Sr_i: dyke 1 has an average value of 0.7046 ± 0.0001, while dykes 4, 5 and 6 have values in the range 0.7054–0.7062 (average values of 0.7059 ± 0.0002, 0.7058 and 0.7056 ± 0.0006, respectively).

Initial $\varepsilon(Nd)$ are positive for all samples and range from +0.6 to +3.1; the highest values are recorded for the porphyritic dykes (+2.0 to +3.1) and the lowest for the aphyric dykes (+0.6 to +1.3) (Fig. 5b). In an $\varepsilon(Nd)_i$–Sr_i binary diagram, data from the Egersund Swarm define a short trend with negative slope (Fig. 5c). This trend starts at the porphyritic dykes with Sr isotopic compositions close to bulk-earth value (0.7037) and depleted Nd compositions ($+2.0 \leq \varepsilon(Nd)_i \leq +3.1$) and ends at the aphyric alkaline dyke 4 in the upper right quadrant of the plot ($\varepsilon(Nd)_i = +1.0$; $Sr_i = 0.7060$).

Differentiation of the Egersund Swarm

Thermomechanical modelling suggests that voluminous basaltic suites in continental environments do not originate by partial melting of the lithospheric mantle (Arndt & Christensen 1992; Anderson 1994), but take place in the asthenospheric mantle. The composition of basaltic products is likely to be dependent on a large number of parameters, including source composition and mineralogy, partial melting conditions, interaction between magmas and lithosphere and crystallization conditions. Understanding the genesis of a rock suite is possible if variations in the magmatic products can be related to individual parameters, the influence of the other ones being either well-defined, negligible or constant. In this context, the relatively small number of dykes in the Egersund Swarm, the absence of primary basaltic magmas and the fragmentary geological record in the late-Neoproterozoic make it difficult to address fundamental and debated questions related to basalt genesis. Nevertheless, some qualitative constraints on the genesis of the Swarm can be extracted from the data.

Phase relations

The most magnesian olivine observed in the swarm is Fo82.5 in porphyritic dyke 11 (Appendix 2), a value largely below the assumed range for mantle peridotites (Fo89–92; e.g. Elthon 1989; Albarède 1992). This indicates that no primary basalt is exposed in the Swarm, and that magmas underwent extensive fractionation before emplacement. The succession and composition of liquidus phases of the most primitive magma composition observed in the Swarm can be estimated using empirical expressions describing mineral–melt equilibrium, and compared to observed early crystallizing phases in the Swarm, i.e. plagioclase, olivine and clinopyroxene. The COMAGMAT program (Ariskin et al. 1993) estimates temperature and crystallizing mineral assemblage for successive crystallization steps. Fractional crystallization starting from sample B224 of porphyritic dyke 3 was modelled using this program for dry conditions along the QFM oxygen buffer (Fig. 2). Different pressures of crystallization were tested, as the position of the olivine–clinopyroxene cotectic is heavily dependent on this variable, the stability field of clinopyroxene being expanded at high pressure (summary in Fram & Lesher 1997). At 1 kbar, COMAGMAT predicts crystallization of plagioclase (An82) at 1225°C, followed by olivine (Fo84) at 1215°C and augite at 1155°C. At 5 and 8 kbar, the crystallizing succession is similar, except that crystallization starts at slightly higher temperatures (1240 and 1250°C, respectively). At 10 kbar, crystallization starts at 1260°C with augite and plagioclase (An80) followed at 1245°C by olivine (Fo83); the narrow temperature interval for crystallization of these three phases indicates that the composition of sample B224 is close to the 10 kbar plagioclase–clinopyroxene–olivine cotectic. The Al_2O_3 content of the clinopyroxene increases with pressure from 2.3% at 1 kbar to 5.8% at 10 kbar.

The composition of the equilibrium crystallizing mineral assemblage predicted at 10 kbar is close to the

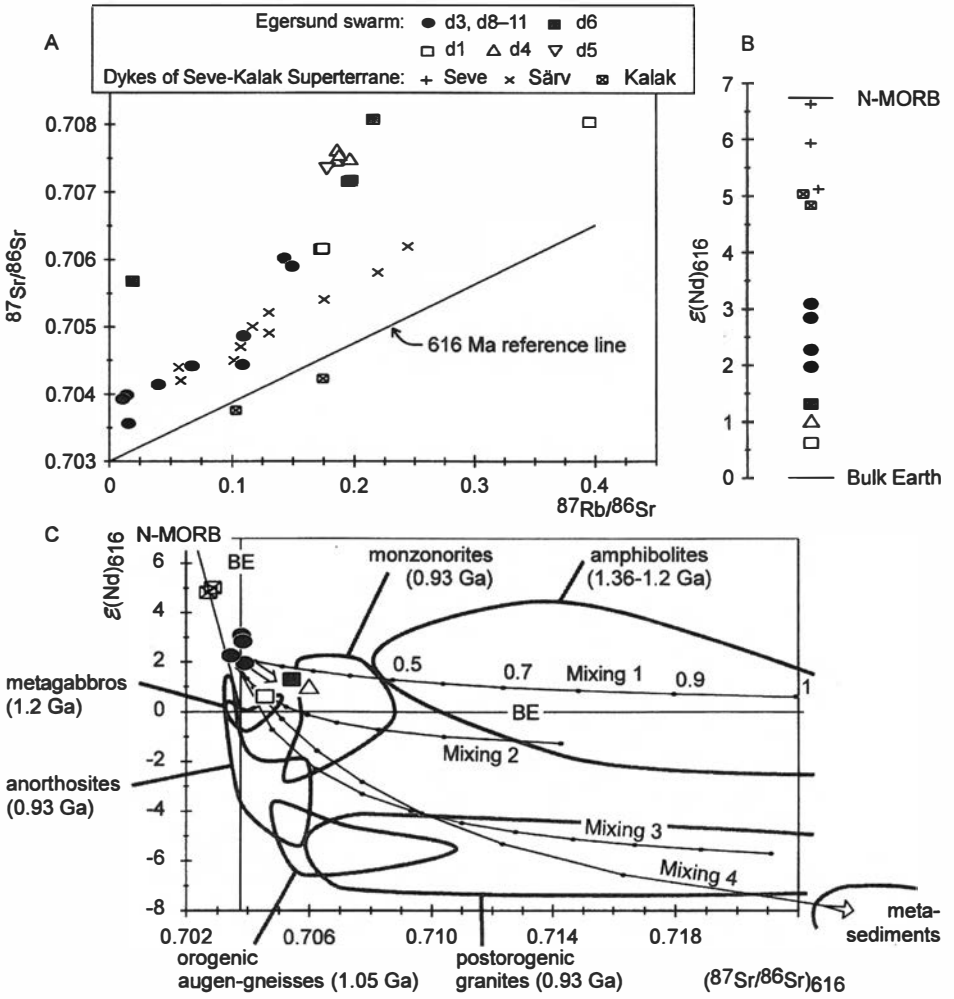

Fig. 5. Isotopic composition of the Egersund Swarm. Comparison with other swarms of the Baltoscandian margin. (A) Whole-rock Rb-Sr data. (B) $\varepsilon(Nd)_i$. Values for MORB and Bulk-Earth (BE) reservoir are shown. (C) $\varepsilon(Nd)_i - Sr_i$ diagram. Isotopic values calculated at 616 Ma for different rock formations from the Sveconorwegian basement of south Norway are plotted (envelope curves displayed by grey curves): Mesoproterozoic metasediments in the amphibolite-to-granulite facies domain of Bamble (Andersen et al. 1995), 1.36–1.2 Ga amphibolite lenses in the Rogaland and Bamble granulite-facies domains (Menuge 1988; Andersen et al. 1995), 1.2 Ga metagabbro bodies (Vestre Dale gabbro; de Haas et al. 1993), 1.05 Ga orogenic calc-alkaline augen gneiss bodies (Bingen et al. 1993), 0.93 Ga postorogenic granite plutons (Herefoss granite; Andersen 1997), 0.93 Ga anorthosite, leuconorite and monzonorite bodies of the Rogaland anorthosite complex (Demaiffe et al. 1986; Menuge 1988; Demaiffe et al. 1990). Mixing hyperbolas (graduated from 0 to 1 with 0.1 increments) between porphyritic dykes (sample B224, dyke 3) and four Sveconorwegian formations are shown for reference. Mixing line 1: average of 6 amphibolites (Sr = 86 ppm, $(^{87}Sr/^{86}Sr)_{616} = 0.7142$, Nd = 30 ppm, $\varepsilon(Nd)_{616} = -1.25$); line 2: average of 2 amphibolites (170, 0.722, 30, +0.6, same parameters, respectively); line 3: average of 13 samples of the post-orogenic Herefoss granite (320, 0.7211, 115, −5.7); line 4: average of 9 metasediments (45, 0.7688, 22, −10.2).

analysed core compositions of most primitive olivine (Fo82.5), plagioclase (An81) and augite ($Al_2O_3 = 6.1$) in porphyritic dykes, except that the predicted Mg content of the clinopyroxene is slightly higher (En 50) than the analysed one (En 46). The temperature estimate for early crystallization of clinopyroxene and olivine at 10 kbar is consistent with the 1250–1180°C interval obtained by Fe-Mg exchange geothermometry between these minerals in porphyritic dyke 11 (Fig. 2). This reasonable match suggests that the modelling of this magma composition is valid. It also suggests that the phenocrysts observed in porphyritic dykes crystallized at a low-crustal level, prior to intrusion of the dykes at shallow level, and that the differentiation took place at ca. 10 kbar, which corresponds approximately to the crust–mantle boundary.

Liquid lines of descent

If the different dykes of the Swarm are tapping a deep magma chamber, their compositions should define a liquid line of descent starting from the most primitive magma composition observed in the Swarm. Compositions of residual liquids derived from the COMAGMAT modelling at 1, 5, 8 and 10 kbar are compared to the actual compositions of dykes for selected combinations of elements in Fig. 6.

Ratios of incompatible elements show only limited variations during fractional crystallization; so, for example, in a Ce/Yb–Yb diagram (Fig. 6a), calculated liquid lines of descent at different pressures are almost horizontal and overlapping (19.7 <Ce/Yb <21.1). In this diagram, aphyric dyke 6 (Ce/Yb = 22.5) lies close to the liquid lines after ca. 40% crystallization, whereas alkaline dykes (d1, d4–d5; 30.8 <Ce/Yb <36.9) are above the fractional crystallization trend. Other combinations of elements yield similar conclusions, namely that dyke 6 is a possible residual product of crystallization of the most primitive magma in porphyritic dykes, whereas high incompatible element contents and distinct incompatible element ratios in alkaline dykes cannot be explained by fractional crystallization of olivine, plagioclase or augite from the most primitive magma at any crustal level. This indicates that the Swarm probably consists of two distinct suites: a subalkaline to mildly alkaline suite represented by porphyritic dykes and dyke 6, and an alkaline suite represented by dykes 1, 4 and 5.

Fractionation of olivine, plagioclase and clinopyroxene

can be tested further using the trends of variably compatible elements in residual liquids, e.g. MgO, CaO/Al_2O_3, Ni, Sc and Sr (Fig. 6b–e). Olivine fractionation results in a strong decrease of MgO, but does not change the CaO/Al_2O_3 ratio. Clinopyroxene fractionation induces MgO and CaO/Al_2O_3 decreases, whereas fractionation of bytownitic plagioclase (CaO/Al_2O_3 of 0.45–0.50) results in an increase in the CaO/Al_2O_3 ratio. Accumulation of these minerals leads to opposite trends. Ni is compatible in olivine, Sc is mildly compatible in clinopyroxene, but incompatible in olivine and plagioclase and Sr is compatible in plagioclase. Thus, residual liquids are depleted in Ni by olivine fractionation, in Sc by clinopyroxene fractionation and in Sr by plagioclase fractionation. Evolution trends in Fig. 6b–e confirm the previous interpretation of the differentiation process on three aspects, as follows:

1. Low-pressure differentiation (1 kbar) with crystallization of plagioclase and olivine and late crystallization of clinopyroxene (after 40% crystallization) results in far-too-large increases in CaO and Sc and a decrease in Sr in residual liquids compared to the range of compositions observed in the mildly alkaline series. The calculated trends at 8 and 10 kbar better describe the data set, although they do not perfectly match the data, especially for Ni. This obviously suggests that the fractional crystallization model is an oversimplification.
2. High Ce and Sr and low Sc contents of the alkaline dykes (d1, d4–5) are not predicted by fractional crystallization of the most primitive magma of the Swarm.
3. The most primitive samples in the porphyritic dykes display limited ranges of Yb, Ce, Sr and Sc contents, but show a significant spread in the CaO/Al_2O_3–MgO diagram, suggesting limited plagioclase accumulation. This is consistent with the interpretation that early crystallized phenocrysts, mainly plagioclase, were carried by the dykes during intrusion and locally accumulated.

The relationship between the alkaline dykes is not clear and is still in abeyance. Dykes 4 and 5 represent a low-Mg#, Si-poor (SiO_2 = 46.1%) highly fractionated magma (Figs. 3, 6). Relating their composition to a specific fractionation history is not straightforward. Dyke 4 has very high P_2O_5 (about 2.5%); it is situated on the experimental apatite saturation curve of Green & Watson (1982) at 1080°C and 7.5 kbar. This suggests that this liquid is saturated in apatite, and is thus probably a multi-saturated magma. Elements classically considered as incompatible could have had compatible behaviour under these circumstances.

Lithospheric assimilation

Geochemical and isotopic signatures of continental basalt suites are commonly attributed to interaction between magma derived from the asthenosphere and continental lithosphere during ascent. The sub-continental lithospheric mantle is geochemically poorly defined and possibly of variable composition (Arndt & Christensen 1992). When modified by metasomatic processes during a paleosubduction event, it probably bears a LILE enriched signature coupled with negative anomalies in Nb, Ta and Ti (e.g. Cadman et al. 1995). In the Sveconorwegian basement of south Norway, there is abundant evidence for Proterozoic plutonic suites enriched in LILE with negative Nb anomaly (e.g. Smalley & Field 1985; de Haas et al. 1993; Bingen & van Breemen 1998). These suites were variably interpreted as directly related to active subduction during the Gothian or Sveconorwegian orogenic periods or as derived from a reservoir modified by subduction-related fluids. It is thus probable that the Sveconorwegian subcontinental lithospheric mantle had a subduction signature. Nevertheless, the Sveconorwegian orogeny ended up with a phase of post-collisional extension at ca. 0.93 Ga, during which the lithospheric mantle may have collapsed (summary in Romer 1996; Bingen et al. 1998a). The geochemical signature of the late-Neoproterozoic lithospheric mantle is thus unknown in the region. The less differentiated magmas of the Egersund Swarm do not display significant Nb, Ta and Ti anomalies, and are thus presumably not modified by a metasomatized continental lithospheric mantle.

The continental crust is highly variable in composition. Except 'depleted' granulite terrains, crustal rocks are generally also enriched in LILE and display negative Nb and Ta anomalies. They are characterized by radiogenic Sr and non-radiogenic Nd. Modelling of Sr, Nd and Pb isotopes in granitoid complexes of the Sveconorwegian basement of south Norway (Andersen et al. 1994; Andersen 1997) does not provide evidence for a widespread LILE 'depleted' granulite-facies lower crustal reservoir, but indicates a lower crust having an 'upper continental crust' type of signature (moderately enriched in LILE) with a Nd depleted mantle model age (t_{DM}) of 1.6–1.9 Ga. If the dykes of the Egersund Swarm were comagmatic, the decrease of $\varepsilon(Nd)_i$ and the increase of the Sr_i from porphyritic to aphyric dykes (Fig. 5c) could suggest that assimilation of this type of crustal material occurred during differentiation and intrusion. Different rock formations from the country rocks were considered potential contaminants (Fig. 5c). At 616 Ma, typical quarzofeldspathic rock units of the Sveconorwegian crust (granitoids and metasediments) have $\varepsilon(Nd)$ in the range −4 to −12, with $^{87}Sr/^{86}Sr$ higher than 0.705. Aphyric dyke 6 and the most alkaline dykes (d4, d5) plot significantly above the hyperbolae, representing mixing lines between these rocks and the porphyritic dykes (mixing lines 3 and 4 of Fig. 5c). These rock units are thus not suitable crustal contaminants. Among the mafic country rocks, only the amphibolite lenses, interlayered in granulite-facies gneiss complexes and older than 1.2 Ga, contain sufficiently radiogenic Sr to be viable contaminants. Assimilation of 20–35% of this material could account for the isotopic

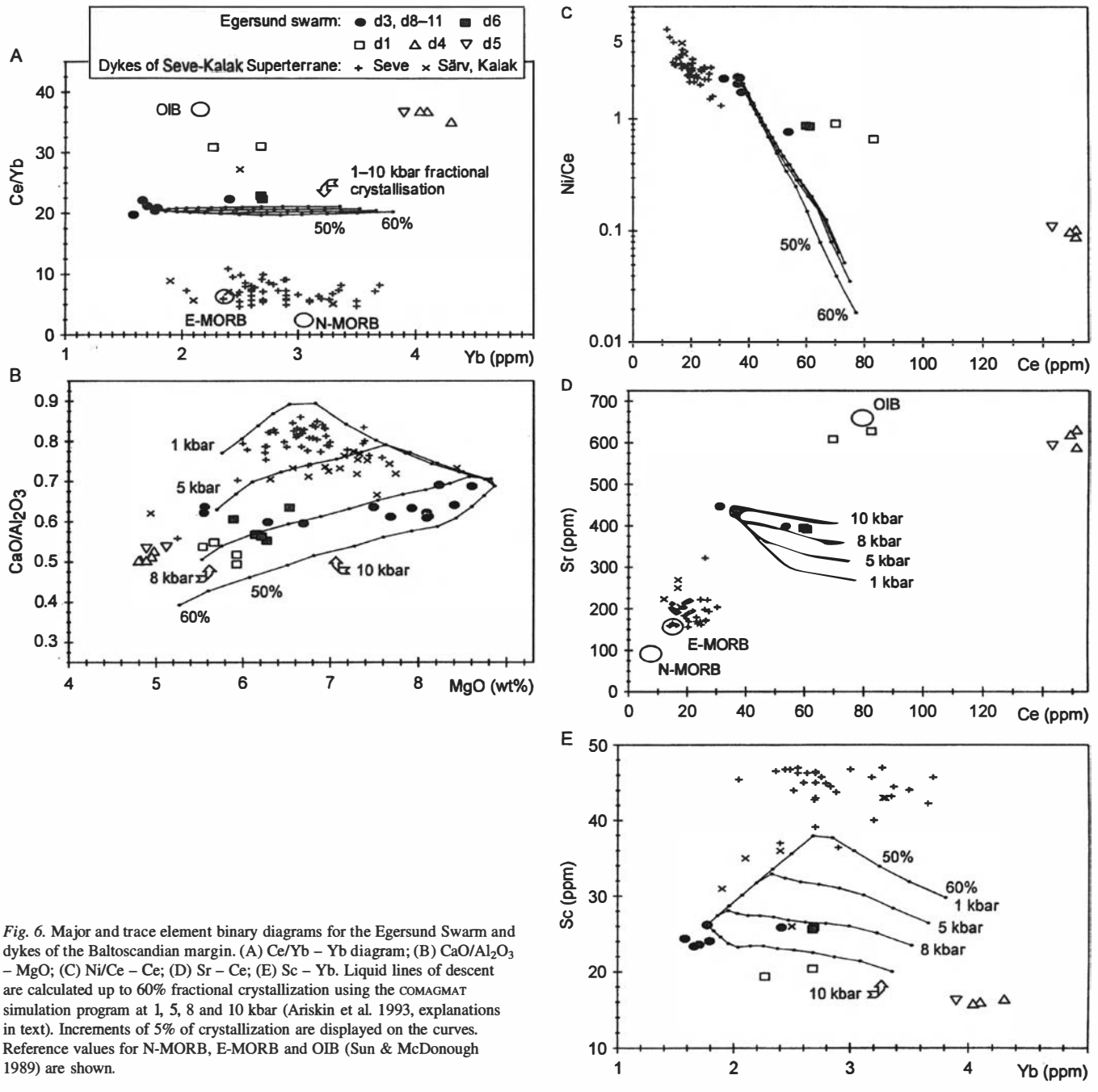

Fig. 6. Major and trace element binary diagrams for the Egersund Swarm and dykes of the Baltoscandian margin. (A) Ce/Yb – Yb diagram; (B) CaO/Al_2O_3 – MgO; (C) Ni/Ce – Ce; (D) Sr – Ce; (E) Sc – Yb. Liquid lines of descent are calculated up to 60% fractional crystallization using the COMAGMAT simulation program at 1, 5, 8 and 10 kbar (Ariskin et al. 1993, explanations in text). Increments of 5% of crystallization are displayed on the curves. Reference values for N-MORB, E-MORB and OIB (Sun & McDonough 1989) are shown.

composition of dyke 6 and alkaline dykes 4 and 5 (mixing lines 1 and 2 of Fig. 5c). These amphibolites could represent a reworked and hydrated middle to lower crust, not depleted in Rb and characterized by a distinctly higher $\varepsilon(Nd)$ ($-4 \leq \varepsilon(Nd) \leq +4$) than the quarzofeldspathic crust ($-12 \leq \varepsilon(Nd) \leq -4$) or the model lower crust of Andersen (1997; $\varepsilon(Nd) < -8$). A comprehensive geochemical data set for these amphibolites is not available, so it is difficult to test properly a specific model of crustal assimilation during fractional crystallization (AFC process).

Nevertheless, published average values of crustal rocks (Rudnick & Fountain 1995) can be used to visualize crustal contamination trends. For example, the Th/Ce and Nb/La ratios, which remain nearly constant during fractional crystallization of major minerals, are sensitive to contamination by crustal material with high Th/Ce and low Nb/La ratios. In Fig. 7 the Th/Ce, Nb/La and Ce/Yb ratios of the Egersund dykes are compared to average values of common amphibolite- to granulite-facies rocks. Dyke 6 has a slightly higher Th/Ce ratio and lower Nb/La ratio than porphyritic dykes of similar Ce/Yb ratio. Its composition thus possibly corresponds with a residual magma of the subalkaline to mildly alkaline suite contaminated by minor amounts of crustal component. Dyke 1 has a similar Th/Ce ratio and slightly lower Nb/La ratio than porphyritic dykes. Its Ce/Yb ratio is, nevertheless, significantly higher

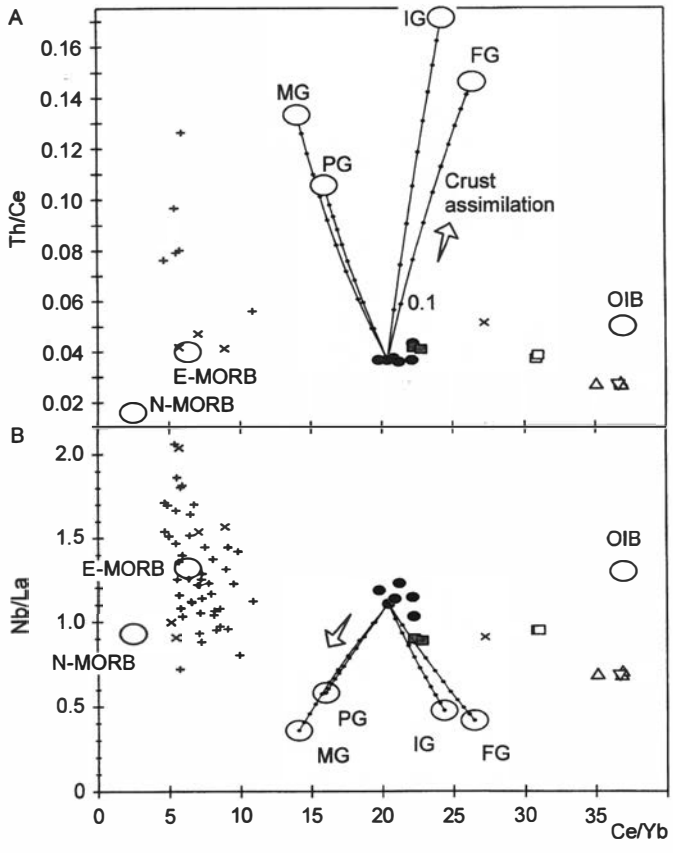

Fig. 7. Test for crustal assimilation. (A) Th/Ce – Ce/Yb diagram; (B) Nb/La – Ce/Yb diagram. Symbols as in Fig. 6. Reference values for N-MORB, E-MORB and OIB (Sun & McDonough 1989) and lower crustal rocks (Rudnick & Fountain 1995) are shown. MG – Mafic granulite, PG – Pelitic granulite, IG – intermediate granulite, FG – felsic granulite. Mixing curves (graduated from 0 to 1 with 0.1 increments) between the most primitive basaltic composition in the Egersund Swarm (d3) and various crustal rocks are shown.

than both porphyritic dykes and crustal material, suggesting that crustal assimilation was not the process responsible for the observed compositional gap between the two suites of the Swarm.

Late-Neoproterozoic rifting in western Baltica

Swarms of the Baltoscandian margin

In the Neoproterozoic Baltoscandian passive margin of Baltica, which is exposed in the Seve–Kalak Superterrane (Roberts & Gale 1978; Andréasson 1994; Andréasson et al. 1998), late-Neoproterozoic basaltic dyke swarms are common in Neoproterozoic sediment sequences. The main swarms are the Ottfjället Swarm in the Särv Nappe complex in Sweden (Solyom et al. 1979) and dykes in the equivalent Leksdal Nappe in Norway (Andréasson et al. 1979), the Sarek swarm in the Sarektjåkkå Nappe (Seve Nappe complex; Andréasson et al. 1992) and correlative dykes in Indre Troms (Rohkunborri Nappe; Stølen 1994) and dykes in the Corrovarre Nappe (Kalak Nappe complex; Roberts 1990). In the Seve Nappe complex, dyke swarms are locally voluminous and form sheeted dyke complexes representing more than 70% of outcrop surface, for example, the Sarek and Rohkunborri dykes. These dyke complexes point to extreme crustal extension and lithospheric thinning (Svenningsen 1995), and correspond to the transition between continental rifting and sea floor spreading in Iapetus (rift-to-drift transition; Svenningsen 1994).

The Ottfjället Swarm is dated at 665 ± 10 Ma (whole-rock K-Ar age; Claesson & Roddick 1983), but is probably younger, as it cuts Varanger Ice Age deposits of 653 ± 7 Ma (Pringle 1973). A dyke in the Corrovarre Nappe yields a Sm-Nd internal isochron age of 582 ± 30 Ma (Zwaan & Van Roermund 1990). The Sarek Swarm is dated at 573 ± 74 Ma by a Sm-Nd internal isochron or 608 ± 1 Ma by zircon U-Pb geochronology (Svenningsen 1994, 1996). If this last zircon age is selected, the opening of Iapetus along the Baltoscandian margin is tightly constrained and occurred shortly (ca. 8 m.y.) after the intrusion of the Egersund Swarm.

Geochemical signatures of the Baltoscandian swarms

Major and trace element data on unaltered and unmetamorphosed fine- to medium-grained dykes are available for the Ottfjället Swarm (Solyom et al. 1979, 1985), the Corrovarre dykes (Roberts 1990), the Sarek Swarm (Andréasson et al. 1992; Svenningsen 1994) and Rohkunborri dykes (Stølen 1994). These different groups have largely overlapping tholeiitic–subalkaline composition, with Mg# of 62–44, TiO_2 content of 1.1–2.4% and SiO_2 content of 47.1–52.3% (Fig. 3a, b). In the binary Zr/TiO_2–Nb/Y diagram, they plot in the field of basalt to subalkaline basalt (Fig. 3d). In major and trace element geotectonic discrimination diagrams, they are in the fields of T-MORB to E-MORB (summary in Andréasson 1994; Andréasson et al. 1998). In normalized multielement diagrams, samples of the Rohkunborri and Sarek dykes are close to typical E-MORB patterns. They show irregularities and enrichments for some of the most incompatible LIL elements (Rb, Ba, Th, K), which is attributed to local upper crustal contamination (Andréasson et al. 1992; see also Fig. 6). In the Ottfjället Swarm of the Särv Nappe complex, there is a minor but significant group of samples with mildly alkaline affinity, characterized by comparatively higher contents in TiO_2 (2.0%), P_2O_5 (0.4%), Zr (ca. 260 ppm), Nb (ca. 30 ppm) and LREE (La = 35 ppm) (Solyom et al. 1979, 1985).

Sr isotopic data are available for the Corrovarre dykes (Zwaan & Van Roermund 1990) and the Ottfjället Swarm (Claesson 1976). These swarms have low Rb content and limited variation of Rb/Sr ratios. Average Sr_i calculated at 610 Ma are 0.7028 ± 0.0002 ($n = 2$) for the Corrovarre samples and 0.7039 ± 0.0003 ($n = 10$) for the Ottfjället samples (Fig. 5a). Nd isotopic data are available for the Corrovarre dykes (Zwaan & Van Roermund 1990) and for the Sarek Swarm (Andréasson et al. 1992; Svenningsen 1994). $\varepsilon(Nd)_i$ range from +4.8 to +6.6. The highest values

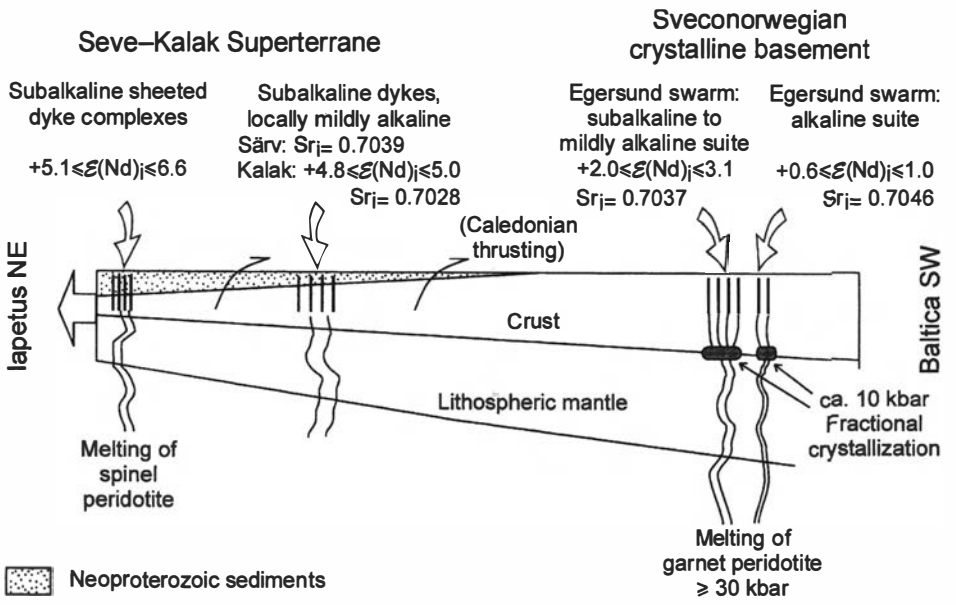

Fig. 8. Schematic interpretative cross-section of the late-Neoproterozoic northwestern passive margin of Baltica. A summary of Sr and Nd isotopic data of the Egersund Swarm and swarms of the Särv, Kalak and Seve Nappe complexes is shown. See text for explanations.

are recorded for the sheeted dyke complexes in the Seve Nappe complex (Fig. 5b).

Mantle sources and paleogeography of Iapetus opening

Although the record of late-Neoproterozoic magmatic products is fragmentary in western Baltica, the first-order 'oceanwards' paleogeographic zonation of the different dyke swarms associated with the opening of Iapetus is correlated with a first-order evolution of geochemical signatures (Andréasson 1994; Andréasson et al. 1998). Starting from the 616 ± 3 Ma Egersund Swarm intruding the crystalline basement of southwest Norway, moving to the swarms intruding the passive margin sedimentary sequences in the Särv and Kalak Nappe complexes, and finishing at the 608 ± 1 Ma sheeted dyke complexes in the Seve Nappe complex attributed to the rift-to-drift transition, there is a decrease in content of most incompatible elements (Figs. 3, 6, 8). This trend is correlated to a decrease in Sr_i (Fig. 5a), and an increase in $\varepsilon(Nd)_i$ value (Fig. 5b). The Egersund Swarm itself comprises two magmatic suites: a subalkaline to mildly alkaline suite and an alkaline suite, the latter being the enriched end of this trend. As shown previously for the Egersund Swarm, the geochemical differences between the two suites cannot be related to fractional crystallization effects and/or crustal assimilation, but must be linked to mantle processes and/or properties.

Two geochemical arguments suggest that the Egersund Swarm could result from partial melting of garnet peridotite with residual garnet, whereas dykes of the Seve Nappe complex could be derived from spinel peridotite. These arguments are as follows:

1. The HREE content in the most primitive dykes of the Egersund Swarm ($3.2 < Yb_N < 3.6$) is significantly lower than in the Seve dykes ($4.1 < Yb_N < 7.5$) (Figs. 3c, 6a), and the slope of the REE pattern is steeper ($5.9 < La_N/Yb_N < 6.9$ and $1.1 < La_N/Yb_N < 3.5$, respectively). HREEs are incompatible in mantle minerals except in garnet; low levels of HREEs in basalt (Yb_N of ca. 4.4) with highly fractionated REE patterns are thus generally attributed to partial melting in the presence of residual garnet.
2. Similarly, Sc contents in the Egersund Swarm (23–26 ppm in the mildly alkaline suite and 16–20 ppm in the alkaline suite) are significantly lower than in the Seve dykes (36–47 ppm). Sc is mildly compatible in clinopyroxene and compatible in garnet; partial melting of peridotite with residual garnet therefore produces melts with low Sc content, typically 20–30 ppm, which is similar to the average level in the Egersund Swarm, whereas partial melting of a spinel peridotite produces high Sc melts, typically 35–50 ppm, similar to the level in the Seve swarms (calculations provided in Saunders et al. 1997).

The differences in mantle sources and processes between the two suites of the Egersund Swarm are difficult to assess precisely, as the alkaline dykes are significantly more evolved. The higher content in incompatible trace elements and the more fractionated REE patterns of the alkaline dykes (Figs. 3c, 6a, 6d) could suggest that they result from a smaller degree of partial melting.

The possible occurrence of residual garnet in the source of the Egersund Swarm implies that partial melting took place at high pressure, probably above 30 kbar, as proposed by Falloon et al. (1988) on the basis of experimental work. Thus, there seems to be a transition in the partial melting conditions associated with the late-Neoproterozoic opening of Iapetus, from high-pressure melting under the continental lithosphere to lower-pressure melting at the continent–ocean transition zone. The continental lithosphere possibly acted as a lid above a

thermal anomaly or mantle plume, truncating the melting column in the asthenospheric mantle and thus limiting the production of magma to high-pressure zones (Fram & Lesher 1997; Saunders et al. 1997) (Fig. 8).

The isotopic data show that the Egersund Swarm is derived from mildly depleted mantle sources at 616 Ma ($0.7037 \leq Sr_i \leq 0.7046$ and $+0.6 \leq \varepsilon(Nd)_i \leq +3.1$), whereas the dykes of the Seve Nappe complex are derived from MORB-type depleted mantle sources ($+5.1 \leq \varepsilon(Nd)_i \leq +6.6$). These differences in isotopic composition indicate that several sources situated in spatially and/or temporally distinct portions of the mantle were sampled. Within the Egersund Swarm itself, the difference in Sr_i and $\varepsilon(Nd)_i$ between the subalkaline to mildly alkaline suite ($Sr_i = 0.7037$ and $+2.0 \leq \varepsilon(Nd)_i \leq +3.1$) and the alkaline suite ($Sr_i = 0.7046$ and $+0.6 \leq \varepsilon(Nd)_i \leq +1.0$) shows that at least two sources were active at local scale to produce this swarm. If the basaltic dykes associated with the Iapetus opening derived from a large mantle plume, as discussed by Andréasson et al. (1998), the isotopic signatures point to significant heterogeneity within such a plume.

Conclusions

The Egersund basaltic dyke swarm intruded the crystalline basement of southwest Norway at 616 ± 3 Ma. New petrological, geochemical and isotopic (Sr, Nd) data allow new constraints to be put on the genesis of this swarm.

Limited differentiation of the magmas occurred in the upper crust, at the intrusion level of the Swarm. The composition of the most primitive magma of the Swarm is close to the clinopyroxene–plagioclase–olivine cotectic calculated at 10 kbar. The crystallizing mineral assemblage, predicted at 10 kbar, reasonably matches the core compositions of the most primitive olivine (Fo82.5), plagioclase phenocryst (An81) and augite ($Al_2O_3 = 6.1$) analysed in porphyritic dykes. This suggests that the magma ponded at the crust–mantle boundary before intrusion at shallow level. Fractional crystallization modelling and assessment of crustal assimilation suggest that the Egersund Swarm consists of two distinct magmatic suites, a subalkaline to mildly alkaline suite and an alkaline suite. The two suites were derived from a slightly depleted asthenospheric mantle source characterized by the following isotopic values: $Sr_i = 0.7037$ and $+2.0 \leq \varepsilon(Nd)_i \leq +3.1$ for the subalkaline to mildly alkaline suite, and $Sr_i = 0.7046$ and $+0.6 \leq \varepsilon(Nd)_i \leq +1.0$ for the alkaline suite. Garnet was a probable residual mineral in the partial melting process.

The Egersund Swarm is part of the late-Neoproterozoic magmatic province of Baltica associated with the opening of the Iapetus Ocean (Andréasson 1994; Andréasson et al. 1998). It displays a geochemical signature significantly more enriched in incompatible trace elements, and is derived from a distinctly less depleted mantle source than slightly younger swarms that are situated in the continent–ocean transition zone. Along the northwestern margin of Baltica, an 'oceanwards' first-order zonation of magmatic products linked to Iapetus opening is thus probably observed.

Acknowledgements. – B. Bingen was 'Chargé de recherches du Fonds National de la Recherche Scientifique de Belgique' when this study was initiated. Thanks are due to C. Chaval, A. Herbosch, C. Leger, J.-P. Mennessier and D. Weis for analytical work or analytical assistance. INAA analyses were carried out by J. Hertogen. T. Andersen, P.-G. Andréasson and T. Grenne are thanked for constructive reviews.

Manuscript received September 1998

References

Albarède, F. 1992: How deep do common basaltic magmas form and differentiate? *Journal of Geophysical Research, 97-B7,* 10997–11009.

Andersen, T. 1997: Radiogenic isotope systematics of the Herefoss granite, South Norway: an indicator of Sveconorwegian (Grenvillian) crustal evolution in the Baltic shield. *Chemical Geology, 135,* 139–158.

Andersen, T., Hagelia, P. & Whitehouse, M. J. 1994: Precambrian multi-stage crustal evolution in the Bamble sector of south Norway: Pb isotopic evidence from a Sveconorwegian deep-seated intrusion. *Chemical Geology (Isotope Geoscience Section), 116,* 327–343.

Andersen, T., Maijer, C. & Verschure, R. H. 1995: Metamorphism, provenance ages, and source characteristics of Precambrian clastic sediments in the Bamble sector, Southern Norway: Ar, Sr, Nd, and Pb isotope study. *Petrology, 3,* 321–339.

Anderson, D. L. 1994: The sublithospheric mantle as the source of continental flood basalts, the case against the continental lithosphere and plume head reservoirs. *Earth and Planetary Science Letters, 123,* 269–280.

Andréasson, P. -G. 1994: The Baltoscandian Margin in Neoproterozoic – early Palaeozoic times. Some constraints on terrane derivation and accretion in the Arctic Scandinavian Caledonides. *Tectonophysics, 231,* 1–32.

Andréasson, P. -G., Solyom, Z. & Roberts, D. 1979: Petrochemistry and tectonic significance of basic and alkaline-ultrabasic dykes in the Leksdal Nappe, northern Trondheim region, Norway. *Norges Geologiske Undersøkelse Bulletin, 348,* 47–71.

Andréasson, P. -G., Svenningsen, O., Johansson, I., Solyom, Z. & Xiaodan, T. 1992: Mafic dyke swarms of the Baltica–Iapetus transition, Seve Nappe Complex of the Sarek Mts., Swedish Caledonides. *Geologiska Föreningens i Stockholm Förhandlingar, 114,* 31–45.

Andréasson, P. -G., Svenningsen, O. M. & Albrecht, L. 1998: Dawn of Phanerozoic orogeny in the North Atlantic tract: evidence from the Seve–Kalak Superterrane, Scandinavian Caledonides. *GFF, 120,* 159–172.

Antun, P. 1955: Géologie et pétrologie des dolérites de la région d'Egersund (Norvège méridionale). *Unpublished thesis, Laboratoire de Pétrologie, Université de Liège, Liège,,* 142.

Ariskin, A. A., Frenkel, M. Y., Barmina, G. S. & Nielsen, R. L. 1993: COMAGMAT: a FORTRAN program to model magma differentiation processes. *Computers and Geosciences, 19,* 1155–1170.

Arndt, N. T. & Christensen, U. 1992: The role of lithospheric mantle in continental flood volcanism: thermal and geochemical constraints. *Journal of Geophysical Research, 97-B7,* 10967–10981.

Bingen, B., Boven, A., Punzalan, L., Wijbrans, J. & Demaiffe, D. 1998a: Hornblende $^{40}Ar/^{39}Ar$ geochronology across terrane boundaries in the Sveconorwegian province of S Norway. *Precambrian Research, 90,* 159–185.

Bingen, B., Demaiffe, D., Hertogen, J., Weis, D. & Michot, J. 1993: K-rich calc-alkaline augen gneisses of Grenvillian age in SW Norway: mingling of mantle-derived and crustal components. *Journal of Geology, 101,* 763–778.

Bingen, B., Demaiffe, D. & van Breemen, O. 1998b: The 616 Ma old Egersund basaltic dike swarm, SW Norway, and late Neoprotorozoic opening of Iapetus ocean. *Journal of Geology, 106,* 565–574.

Bingen, B. & van Breemen, O. 1998: Tectonic regimes and terrane boundaries in the high-grade Sveconorwegian belt of SW Norway, inferred from U-Pb zircon geochronology and geochemical signature of augen gneiss suites. *Journal of the Geological Society, London, 155,* 143–154.

Cadman, A. C., Tarney, J. & Baragar, W. R. A. 1995: Nature of mantle source contributions and the role of contamination and *in situ* crystallisation in the petrogenesis of Proterozoic mafic dykes and flood basalts, Labrador. *Contributions to Mineralogy and Petrology, 122,* 213–229.

Claesson, S. 1976: The age of the Ottfjället dolerites of Särv Nappe, Swedish

Caledonides. *Geologiska Föreningens i Stockholm Förhandlingar, 98,* 370–374.

Claesson, S. & Roddick, J. -C. 1983: $^{40}Ar/^{39}Ar$ data on the age and metamorphism of the Ottfjället dolerite, Särv Nappe, Swedish Caledonides. *Lithos, 16,* 61–73.

Dalziel, I. W. D. 1997: Neoproterozoic-Paleozoic geography and tectonics: reviews, hypothesis, environmental speculations. *Geological Society of America Bulletin, 109,* 16–42.

de Haas, G. -J., Verschure, R. H. & Maijer, C. 1993: Isotopic constraints on the timing of crustal accretion of the Bamble Sector, Norway, as evidenced by coronitic gabbros. *Precambrian Research, 64,* 403–417.

Demaiffe, D., Bingen, B., Wertz, P. & Hertogen, J. 1990: Geochemistry of the Lyngdal hyperites (SW Norway): comparison with the monzonorites associated with the Rogaland anorthosite complex. *Lithos, 24,* 237–250.

Demaiffe, D., Weis, D., Michot, J. & Duchesne, J. -C. 1986: Isotopic constraints on the genesis of the Rogaland anorthositic suite (SW Norway). *Chemical Geology, 57,* 167–179.

Elthon, D. 1989: Pressure of origin of primary mid-ocean ridge basalts. *In* Saunders, A. D. & Norry, M. J. (eds): *Magmatism in the Ocean Basins*, 125–136. *Geological Society of London Special Publication 42.* Blackwell, Oxford.

Ernst, R. E. & Buchan, K. L. 1997: Giant radiating dyke swarms: their use in identifying pre-Mesozoic large igneous provinces and mantle plumes. *In* Mahoney, J. J. & Coffi, M. F. (eds): *Large Igneous Provinces: Continental, Oceanic, and Planetary Flood Volcanism*, 297–333. *Geophysical Monograph 100.* American Geophysical Union, Washington.

Falloon, T. J., Green, D. H., Hatton, C. J. & Harris, K. L. 1988: Anhydrous partial melting of a fertile and depleted peridotite from 2 to 30 kb and application to basalt petrogenesis. *Journal of Petrology, 29,* 1257–1282.

Fram, M. S. & Lesher, C. E. 1997: Generation of polybaric differentiation of east Greenland early Tertiary flood basalts. *Journal of Petrology, 38,* 231–275.

Green, T. H. & Watson, E. B. 1982: Crystallization of apatite in natural magmas under high pressure, hydrous conditions, with particular reference to 'orogenic' rock series. *Contributions to Mineralogy and Petrology, 79,* 96–105.

Karlsen, T. A., Nilsson, L. P., Schiellerup, H., Marker, M. & Gautneb, H. 1998: Berggrunnsgeologisk kart over Åna-Sira anorthosittmassiv med omgivelser, 1:25000. *Norges geologiske undersøkelse, Trondheim.*

Kumpulainen, R. & Nystuen, J. P. 1985: Late Proterozoic basin evolution and sedimentation in the westernmost part of Baltoscandia. *In* Gee, D. G. & Sturt, B. A. (eds): *The Caledonide Orogen – Scandinavia and Related Areas*, 213–232. John Wiley & Sons, Chichester.

Lindsley, D. H. & Frost, B. R. 1992: Equilibria among Fe-Ti oxides, pyroxenes, olivine, and quartz: part 1, theory. *American Mineralogist, 77,* 987–1003.

Loucks, R. R. 1996: A precise olivine-augite Mg-Fe-exchange geothermometer. *Contributions to Mineralogy and Petrology, 125,* 140–150.

Maijer, C. & Verschure, R. H. 1998: Petrology and isotope geology of the Hunnedalen monzonoritic dyke swarm, SW Norway: a possible late expression of Egersund anorthosite magmatism. *Norges geologiske undersøkelse Bulletin, 434,* 83–107.

Menuge, J. F. 1988: The petrogenesis of massif anorthosites: a Nd and Sr isotopic investigation of the Proterozoic of Rogaland-Vest Agder, SW Norway. *Contributions to Mineralogy and Petrology, 98,* 363–373.

Miller, C. A., Barton, M., Sundvoll, B., Edwards, K. J., Gilliam, C. E. & Valley, J. W. 1996: New age and isotopic data for the Egersund Dolerite, SW Norway: evidence for Iapetus plume-initiated rifting during the Late Precambrian. *EOS, 77,* S277.

Pasteels, P., Demaiffe, D. & Michot, J. 1979: U-Pb and Rb-Sr geochronology of the eastern part of the south Rogaland igneous complex, southern Norway. *Lithos, 12,* 199–208.

Pedersen, R. B. & Hertogen, J. 1990: Magmatic evolution of the Karmoy ophiolite complex, SW Norway: relationships between MORB–IAT–boninite–calk-alkaline and alkaline magmatism. *Contributions to Mineralogy and Petrology, 104,* 277–293.

Pringle, I. R. 1973: Rb-Sr age determinations on shales associated with the Varanger Ice Age. *Geological Magazine, 109,* 465–472.

Roberts, D. 1990: Geochemistry of mafic dykes in the Corrovarre Nappe, Troms, North Norway. *Norges geologiske undersøkelse Bulletin, 419,* 45–53.

Roberts, D. & Gale, G. H. 1978: The Caledonian–Appalachian Iapetus ocean. *In* Tarling, D. H. (ed): *Evolution of the Earth's Crust*, 255–342. Academic Press, London.

Romer, R. L. 1996: Contiguous Laurentia and Baltica before the Grenvillian-Sveconorwegian orogeny? *Terra Nova, 8,* 173–181.

Rudnick, R. L. & Fountain, D. M. 1995: Nature and composition of the continental crust: a lower crustal perspective. *Reviews of Geophysics, 33,* 267–309.

Saunders, A. D., Fitton, J. G., Kerr, A. C., Norry, M. J. & Kent, R. W. 1997: The North Atlantic Igneous Province. *In* Mahoney, J. J. & Coffin, M. F. (eds): *Large Igneous Provinces: Continental, Oceanic, and Planetary Flood Volcanism*, 45–94. *Geophysical Monograph 100.* American Geophysical Union, Washington.

Schärer, U., Wilmart, E. & Duchesne, J. -C. 1996: The short duration and anorogenic character of anorthosite magmatism: U-Pb dating of the Rogaland complex, Norway. *Earth and Planetary Science Letters, 139,* 335–350.

Smalley, P. C. & Field, D. 1985: Geochemical constraints on the evolution of the Proterozoic continental crust in southern Norway (Telemark sector). *In* Tobi, A. C. & Touret, J. L. (eds): *The Deep Proterozoic Crust in the North Atlantic Provinces*, 551–566. Reidel, Dordrecht.

Solyom, Z., Andréasson, P. -G. & Johansson, I. 1985: Petrochemistry of late Proterozoic rift volcanism in Scandinavia: the Särv Dolerites – volcanism in the constructive arms of Iapetus. *Lund Publications in Geology, 35,* 1–42.

Solyom, Z., Gorbatschev, R. & Johanson, I. 1979: The Ottfjäll dolerites: geochemistry of the dyke swarm in relation to the geodynamics of the Caledonide orogen of Central Scandinavia. *Sveriges Geologiska Undersökning, C756,* 1–38.

Stølen, L. K. 1994: Derivation of mafic dyke swarms in the Rohkunborri Nappe, Indre Troms, northern Norwegian Caledonides: geochemical constraints. *GFF, 116,* 121–131.

Sun, S. S. & McDonough, W. F. 1989: Chemical and isotopic systematics of oceanic basalts: implications for mantle composition and processes. *In* Saunders, A. D. & Norry, M. J. (eds): *Magmatism in the Ocean Basins*, 313–345. *Geological Society of London Special Publication 42.* Blackwell, Oxford.

Sundvoll, B. 1987: The age of the Egersund dyke-swarm, SW Norway: some tectonic implications. *Terra Cognita, 7,* 180.

Svenningsen, O. M. 1994: The Baltica-Iapetus passive margin dyke complex in the Sarektjåkkå Nappe, northern Swedish Caledonides. *Geological Journal, 29,* 323–354.

Svenningsen, O. M. 1995: Extensional deformation along the Late Precambrian–Cambrian Baltoscandian passive margin: the Sarektjåkkå Nappe, Swedish Caledonides. *Geologische Rundschau, 84,* 649–664.

Svenningsen, O. M. 1996: Passive margins – past and (almost) present. *GFF, 118,* A41.

Torsvik, T. H. 1998: Palaeozoic palaeogeography: a North Atlantic viewpoint. *GFF, 120,* 109–118.

Torsvik, T. H., Smethurst, M. A., Meert, J. G., Van der Voo, R., McKerrow, W. S., Brasier, M. D., Sturt, B. A. & Walderhaug, H. J. 1996: Continental break up and collision in the Neoproterozoic and Paleozoic – a tale of Baltica and Laurentia. *Earth Science Reviews, 40,* 229–258.

Venhuis, G. J. & Barton, M. 1986: Major element chemistry of Precambrian dolerite dikes of tholeiitic composition from Rogaland/Vest Agder, SW Norway. *Norsk Geologisk Tidsskrift, 66,* 277–294.

Verschure, R. H., Andriessen, P. A. M., Boelrijk, N. A. M., Hebeda, E. H., Maijer, C., Priem, H. N. A. & Verdurmen, E. A. T. 1980: On the thermal stability of Rb-Sr and K-Ar biotite systems: evidence from coexisting Sveconorwegian (ca. 870 Ma) and Caledonian (ca. 400 Ma) biotites in SW Norway. *Contributions to Mineralogy and Petrology, 74,* 245–252.

Vidal, G. & Moczydlowska, M. 1995: The Neoproterozoic of Baltica – stratigraphy, palaeobiology and general geological evolution. *Precambrian Research, 73,* 197–216.

Walderhaug, H. J., Torsvik, T. H., Sundvoll, B., Eide, E. A. & Bingen, B.: Geochronology and palaeomagnetism of the Hunnedalen dykes, SW Norway: the demise of the Sveconorwegian apparent polar wander loop. *Earth and Planetary Science Letters,* in press.

Weis, D., Demaiffe, D., Cauet, S. & Javoy, M. 1987: Sr, Nd, O and H isotopic ratios in Ascension Island lavas and plutonic inclusions: cogenetic origin. *Earth and Planetary Science Letters, 82,* 255–268.

Winchester, J. A. & Floyd, P. A. 1977: Geochemical discrimination of different magma series and their differentiation products using immobile elements. *Chemical Geology, 20,* 325–343.

Wood, D. A. 1980: The application of a Th–Hf–Ta diagram to problems of tectonomagmatic classification and to establishing the nature of crustal contamination of basaltic lavas of the British tertiary volcanic province. *Earth and Planetary Science Letters, 50,* 11–30.

Zwaan, B. K. & Van Roermund, L. M. 1990: A rift-related mafic dyke swarm in the Corrovarre Nappe of the Caledonian Middle Allochthon, Troms, North Norway, and its tectonometamorphic evolution. *Norges geologiske undersøkelse Bulletin, 419,* 25–44.

Appendix 1. Selected microprobe analyses of plagioclase.

Sample	B348	B224	B235	B245	B367	B247	B247	B365	B365	D103	D103
Dyke	d1	d3	d4	d6	d8	d8	d8	d9	d9	d11	d11
Phenocryst[a]						Ph		Ph		Ph	
Analysis	124	86	6	205	180	152	154	240	221	122	112
SiO_2 (wt%)	55.30	51.16	55.84	51.76	52.40	48.05	48.68	46.71	48.58	48.64	52.53
TiO_2	0.11	0.04	0.07	0.06	0.17	0.00	0.06	0.02	0.08	0.00	0.08
Al_2O_3	27.30	29.67	26.41	29.98	28.65	32.58	32.05	32.96	31.87	32.02	28.83
FeO	0.37	0.82	0.42	0.75	0.98	0.39	0.54	0.37	0.55	0.51	0.74
MgO	0.01	0.16	0.04	0.09	0.19	0.14	0.16	0.21	0.20	0.16	0.12
CaO	8.90	12.44	8.37	12.89	11.18	15.33	14.48	16.42	14.76	14.84	11.64
Na_2O	6.09	4.35	6.06	4.35	5.16	2.45	2.99	2.11	3.00	2.92	4.84
K_2O	0.50	0.21	0.98	0.32	0.34	0.10	0.15	0.07	0.09	0.16	0.31
Sum	98.58	98.85	98.19	100.20	99.07	99.04	99.11	98.87	99.13	99.25	99.09
Si[b]	2.526	2.359	2.562	2.431	2.409	2.220	2.246	2.171	2.244	2.244	2.411
Ti	0.004	0.002	0.002	0.005	0.006	0.000	0.002	0.001	0.003	0.000	0.003
Al	1.470	1.613	1.428	1.541	1.552	1.774	1.743	1.806	1.735	1.741	1.559
Fe	0.014	0.032	0.016	0.019	0.038	0.015	0.021	0.014	0.021	0.020	0.028
Mg	0.001	0.110	0.003	0.007	0.013	0.010	0.011	0.015	0.014	0.011	0.008
Ca	0.436	0.615	0.411	0.549	0.551	0.759	0.716	0.818	0.730	0.734	0.572
Na	0.540	0.389	0.539	0.452	0.460	0.220	0.268	0.190	0.269	0.262	0.430
K	0.029	0.013	0.057	0.024	0.020	0.006	0.009	0.004	0.005	0.009	0.018
Ab	53.7	38.3	53.5	44.1	44.6	22.3	27.0	18.8	26.8	26.0	42.2
Or	2.9	1.2	5.7	2.4	2.0	0.6	0.9	0.4	0.5	0.9	1.8
An	43.4	60.5	40.8	53.6	53.5	77.1	72.1	80.8	72.7	73.1	56.1

Note: Analyses obtained with the CAMEBAX microprobe of the CAMST (UCL, Louvain-la-Neuve, Belgium); conditions: 15 kV, 15 na; standardization using oligoclase for Na Kα, leucite for K Kα, hematite for Fe Kα, fayalite for Si Kα, olivine for Mg Kα, wollastonite for Ca Kα, rhodonite for Mn Kα, sapphirine for Al Kα, rutile for Ti Kα and chromite for Cr Kα.

[a] Ph: centre of phenocryst, other analyses: matrix plagioclase.

[b] Formula on the basis of 8 oxygens.

Appendix 2. Selected microprobe analyses of olivine.

Sample	B235	B367	B247	D103
Dyke	d4	d8	d8	d11
Analysis	2	173	62	118
SiO_2 (wt%)	34.28	36.46	39.29	39.33
FeO	42.86	32.00	16.64	16.29
MnO	0.68	0.44	0.19	0.21
MgO	21.84	31.05	44.07	43.48
CaO	0.20	0.17	0.21	0.22
Sum	99.86	100.12	100.40	99.53
Si[a]	0.994	0.994	0.988	0.998
Fe^{2+}	1.039	0.729	0.350	0.346
Mn	0.017	0.010	0.004	0.005
Mg	0.944	1.262	1.652	1.645
Ca	0.006	0.005	0.006	0.006
Sum	3.000	3.000	3.000	3.000
Fo	47.6	63.4	82.5	82.6
Fa	52.4	36.6	17.5	17.4

[a] Formula on the basis of 4 oxygens calculated using subroutine of QUILF program (Lindsley & Frost 1992).

Appendix 3. Selected microprobe analyses of clinopyroxene.

Sample	B348	B224	B235	B245	B367	B365	D103
Dyke	d1	d3	d4	d6	d8	d9	d11
Analysis	127	84	10	202	176	223	107
SiO_2 (wt%)	49.35	48.18	50.47	50.32	48.96	48.55	48.72
TiO_2	1.69	1.89	1.05	0.92	1.53	1.53	1.66
Al_2O_3	3.66	6.1	2.06	2.21	4.37	4.08	5.34
Cr_2O_3	0.06	0.33	0.03	0.03	0.01	0.06	0.04
FeO	10.89	8.17	13.99	13.55	12.1	12	8.5
MnO	0.26	0.14	0.42	0.33	0.34	0.24	0.19
MgO	13.78	14.93	13.02	16.22	14.04	13.72	15.16
CaO	18.99	19.35	17.7	15.78	17.97	18.72	19.01
Na_2O	0.58	0.38	0.65	0.46	0.35	0.48	0.47
Sum	99.26	99.47	99.39	99.82	99.67	99.38	99.09
Si[a]	1.857	1.789	1.915	1.885	1.838	1.828	1.814
Ti	0.048	0.053	0.030	0.026	0.043	0.043	0.046
Al	0.162	0.267	0.092	0.098	0.193	0.181	0.234
Cr^{3+}	0.002	0.010	0.001	0.001	0.000	0.002	0.001
Fe^{3+}	0.069	0.067	0.064	0.078	0.069	0.109	0.078
Fe^{2+}	0.273	0.187	0.380	0.346	0.311	0.268	0.187
Mn	0.008	0.004	0.014	0.010	0.011	0.008	0.006
Mg	0.773	0.826	0.737	0.906	0.786	0.770	0.841
Ca	0.765	0.770	0.720	0.633	0.723	0.755	0.758
Na	0.042	0.027	0.048	0.033	0.025	0.035	0.034
Sum	4.000	4.000	4.000	4.017	4.000	4.000	4.000
Wo	42.3	43.2	39.2	33.6	39.7	42.1	42.4
En	42.7	46.4	40.1	48.0	43.2	42.9	47.1
Fs	15.1	10.5	20.7	18.4	17.1	15.0	10.5

[a] Formula on the basis of 6 oxygens calculated using subroutine of QUILF program (Lindsley & Frost 1992).

Appendix 4. Selected microprobe analyses of titano-magnetite and hemo-ilmenite.

Sample	B348	B348	B224	B224	B235	B235	B245	B245	B367	B367	D103	D103
Dyke	d1	d1	d3	d3	d4	d4	d6	d6	d8	d8	d11	d11
Mineral	Spl	Ilm	Spl	Ilm	Spl	Ilm	Spl	Ilm	Spl	Ilm	Spl	Ilm
Analysis[a]	131	133	82	80	14	13, 15	211	209, 210	167	166	114, 116	115, 117
TiO_2	15.76	48.60	11.21	45.89	18.63	48.87	17.43	49.82	20.65	48.38	20.05	46.30
Al_2O_3	2.38	0.11	0.17	0.08	1.49	0.14	1.66	0.10	2.49	0.12	2.44	0.15
FeO	76.65	48.21	80.95	48.74	74.03	47.19	75.78	48.59	72.30	48.36	70.90	51.28
MnO	0.67	1.30	0.11	2.61	0.56	0.55	0.23	0.58	0.37	0.44	0.22	0.54
MgO	0.05	0.19	0.03	0.12	0.00	1.25	0.02	0.41	0.22	0.19	0.06	0.05
Sum	95.51	98.41	92.47	97.44	94.71	98.00	95.12	99.50	96.03	97.49	93.67	98.32
Ti[a]	0.448	0.933	0.331	0.888	0.538	0.934	0.500	0.945	0.585	0.937	0.583	0.888
Al	0.106	0.003	0.008	0.002	0.067	0.004	0.075	0.003	0.111	0.004	0.111	0.005
Fe^{3+}	0.998	0.132	1.331	0.222	0.857	0.128	0.926	0.108	0.718	0.122	0.722	0.219
Fe^{2+}	1.424	0.897	1.325	0.826	1.520	0.875	1.491	0.917	1.561	0.921	1.573	0.875
Mn	0.021	0.028	0.004	0.057	0.018	0.012	0.007	0.012	0.012	0.010	0.007	0.012
Mg	0.003	0.007	0.002	0.005	0.000	0.047	0.001	0.015	0.012	0.007	0.003	0.002
Sum	3.000	2.000	3.000	2.000	3.000	2.000	3.000	2.000	3.000	2.000	3.000	2.000
Usp	46.7		33.1		55.2		51.7		61.7		61.6	
Mt	53.3		66.9		44.8		48.3		38.3		38.4	
Ilm		93.2		88.2		93.2		94.5		93.8		88.9
Hem		6.8		11.8		6.8		5.5		6.2		11.1

[a] Grains of Spl and Ilm in close proximity but not in contact; single spot analysis or average of two spots.
[b] Formula on the basis of 3 oxygens for Ilm and 4 oxygens for Spl, calculated using subroutine of QUILF program (Lindsley & Frost 1992).

Appendix 5. Selected microprobe analyses of biotite.

Sample	B348	B235	B367
Dyke	d1	d4	d8
Analysis	138	4	181
SiO_2 (wt%)	35.86	37.41	35.87
TiO_2	4.72	4.73	4.61
Al_2O_3	12.67	12.37	11.92
Cr_2O_3	0.04	0.03	0.00
FeO	23.69	19.13	23.82
MnO	0.09	0.06	0.06
MgO	9.62	13.03	8.96
Na_2O	0.17	0.34	0.33
K_2O	9.66	9.13	8.59
H_2O[a]	3.49	3.60	3.43
Sum	100.01	99.83	97.59
Si[b]	5.563	5.657	5.681
Ti	0.550	0.538	0.549
Al	2.317	2.205	2.225
Cr^{3+}	0.004	0.004	0.000
Fe^{2+}	3.074	2.419	3.155
Mn	0.012	0.008	0.007
Mg	2.223	2.937	2.116
Na	0.052	0.100	0.101
K	1.912	1.762	1.737
OH	4.000	4.000	4.000

[a] Calculated value.
[b] Formula on the basis of 22 oxygens.

Appendix 6. Sample locations and whole-rock XRF analyses of Ti, Na, K, P, Ni, Rb, Sr, Y, Zr and Nb.

Sample	B214	B217	B218	B219	B220	B348	B351	B355	B221	B224	B227	B233
Dyke	d1	d1	d1	d1	d1	d1	d1	d1	d3	d3	d3	d4
m/c[a]	c	m	c	c	m	c	c	c	m	c	m	m
Phenocrysts	–	–	–	–	–	–	–	–	–	–	–	–
UTM – x[b]	545	445	445	445	445	377	377	377	250	250	250	401
UTM – y	942	978	978	978	978	994	994	994	853	853	853	763
TiO_2 (wt%)	2.93	3.22	2.99	2.78	3.08	3.00	3.05	3.14	1.99	1.99	1.88	3.45
Na_2O	2.24	2.61	2.48	2.53	2.55	3.02	2.87	2.88	1.88	1.79	1.89	3.01
K_2O	1.32	1.53	1.69	1.64	1.40	1.85	1.31	1.51	0.26	0.24	0.07	2.29
P_2O_5	0.71	0.54	0.71	0.67	0.54	0.76	0.72	0.75	0.30	0.29	0.25	2.42
Ni (ppm)	56	48	60	64	55	55	53	57	84	86	102	16
Rb	31	49	58	83	60	38	34	36	2	2	0	40
Sr	582	576	601	608	510	628	560	596	401	428	437	589
Y	35	35	33	32	35	35	36	34	24	23	22	60
Zr	212	216	205	194	214	217	213	217	153	148	144	295
Nb	35	36	33	31	36	35	34	35	18	17	17	45

Sample	B234	B235	B236	B375	B376	B377	B403	B404	B230	B231	B211	B244
Dyke	d4	d4	d4	d4	d4	d4	d4	d4	d5	d5	d6	d6
m/c[a]	c	c	c	m	c	m	c	c	m	c	m	c
Phenocrysts	–	–	–	–	–	–	–	–	–	–	–	–
UTM – x[b]	401	401	401	263	263	263	401	401	257	257	286	457
UTM – y	763	763	763	821	821	821	763	763	808	808	757	712
TiO_2 (wt%)	3.23	3.20	3.17	3.25	3.19	3.22	3.29	3.14	3.39	3.24	2.27	2.16
Na_2O	3.63	3.70	3.69	3.80	3.76	3.77	2.81	3.67	2.94	3.06	2.81	2.62
K_2O	2.49	2.50	2.53	2.49	2.48	2.48	2.38	2.55	2.19	2.20	0.37	0.62
P_2O_5	2.54	2.50	2.50	2.50	2.47	2.52	2.46	2.55	2.04	2.34	0.26	0.33
Ni (ppm)	13	13	13	13	15	13	15	13	17	16	54	49
Rb	41	41	41	40	40	39	41	41	37	36	4	8
Sr	620	632	626	622	620	624	598	623	589	593	398	367
Y	61	61	60	62	61	61	62	62	59	58	31	32
Zr	301	296	297	295	297	300	300	299	291	287	212	225
Nb	46	46	46	47	47	47	46	47	43	42	24	24

Sample	B245	B338a	B338a	B338b	B339	B339	B340a	B340b	B341	B342	B343	B344
Dyke	d6	d6	d6	d6	d6	d6	d6	d6	d6	d6	d6	d6
m/c[a]	c	m	m	m	m	m	c	c	c	m	c	c
Phenocrysts	–	–	–	–	–	–	+	+	+	–	–	–
UTM – x[b]	457	332	332	332	332	332	332	332	332	332	332	332
UTM – y	712	741	741	741	741	741	741	741	741	741	741	741
TiO_2 (wt%)	2.10	2.22	2.20	2.19	2.21	2.21	2.21	2.23	2.21	2.21	2.08	2.08
Na_2O	3.08	2.61	2.64	2.78	2.54	2.56	2.66	2.69	2.72	2.72	3.11	3.13
K_2O	1.42	0.74	0.74	0.85	0.79	0.79	0.99	1.02	0.87	0.83	1.39	1.38
P_2O_5	0.31	0.27	0.27	0.24	0.28	0.27	0.27	0.26	0.30	0.23	0.32	0.32
Ni (ppm)	52	55	56	55	54	54	55	55	47	55	51	52
Rb	27	15	16	17	16	17	20	21	16	14	26	25
Sr	394	390	390	382	392	392	373	371	388	379	387	391
Y	31	31	31	31	31	31	31	31	34	30	33	32
Zr	232	212	214	209	209	212	214	211	242	204	229	233
Nb	24	25	24	24	24	24	24	24	25	24	25	24

Sample	B345	B347	B372a	B372b	B373	B380	B381	B426	B427	B246	B247	B367
Dyke	d6	d6	d6	d6	d6	d6	d6	d6	d6	d8	d8	d8
m/c[a]	c	c	m	m	c	c	c	m	c	c	c	c
Phenocrysts	–	–	–	–	–	–	–	–	–	+	–	+
UTM – x[b]	332	332	548	548	548	309	309	~494	~494	438	438	465
UTM – y	741	741	675	675	675	744	744	~693	~693	663	663	655
TiO_2 (wt%)	2.06	2.13	2.18	2.17	2.16	2.19	2.13	2.20	2.06	2.10	2.13	2.44
Na_2O	3.11	2.72	2.54	2.72	2.73	2.30	3.19	2.64	2.73	1.86	2.23	2.56
K_2O	1.38	0.83	1.14	1.11	2.36	0.28	1.14	0.86	1.34	0.52	0.60	1.01
P_2O_5	0.34	0.35	0.26	0.22	0.34	0.32	0.33	0.32	0.30	0.27	0.26	0.36
Ni (ppm)	52	49	54	54	52	53	53	54	53	55	65	41
Rb	26	16	23	24	28	2	20	17	25	8	10	20
Sr	391	401	369	364	380	366	384	393	402	410	437	399
Y	32	32	30	31	31	31	33	31	32	23	24	31
Zr	228	231	206	208	209	204	228	205	215	147	158	205
Nb	24	25	24	25	24	25	26	24	24	17	18	23

Appendix 6. Continued.

Sample	B368	B370	B371	B365	B366	D1773	B360	D103
Dyke	d8	d8	d8	d9	d9	d9	d10	d11
m/c[a]	c	m	c	c	c	c	c	c
Phenocrysts	+	+	+	+	+	+	+	+
UTM – x[b]	465	463	463	545	545	~621	545	~55
UTM – y	655	649	649	617	617	~607	605	~58
TiO_2 (wt%)	2.45	2.96	2.93	1.72	1.67	1.97	2.01	1.76
Na_2O	2.58	2.70	2.66	2.02	2.02	2.19	1.56	1.98
K_2O	1.02	0.91	0.96	0.45	0.50	0.68	0.23	0.82
P_2O_5	0.36	0.41	0.42	0.25	0.24	0.24	0.27	0.30
Ni (ppm)	41	39	40	72	80	67	75	86
Rb	21	16	15	6	8	15	2	16
Sr	398	401	401	447	444	402	440	425
Y	31	35	35	21	20	24	23	22
Zr	207	244	241	126	125	140	148	141
Nb	24	28	28	16	16	18	19	18

[a] c: centre of the dyke; m: <30cm margin.
[b] All samples are in UTM zone 32V LK.

Appendix 7. Whole-rock major element analyses.

Sample	B217	B355	B221	B227	B375	B377	B230	B244	B347	B373	B380	B368	B370	B371	B366	D1773
Dyke	d1	d1	d3	d3	d4	d4	d5	d6	d6	d6	d6	d8	d8	d8	d9	d9
SiO_2 (wt%)	46.5	46.9	46.9	46.2	46.2	46.0	45.2	49.6	49.8	49.3	48.8	46.7	47.4	47.5	47.0	47.3
TiO_2	3.22	3.14	1.99	1.88	3.25	3.22	3.39	2.16	2.13	2.16	2.19	2.45	2.96	2.93	1.67	1.97
Al_2O_3	14.94	15.38	16.09	16.25	14.26	14.31	14.21	15.36	15.40	15.36	15.23	15.22	14.71	14.87	17.56	16.26
Fe_2O_3	3.63	3.73	2.84	2.69	3.91	4.04	3.41	2.48	2.63	2.77	2.28	2.93	4.25	4.23	2.84	2.76
FeO	9.29	9.19	7.41	7.17	10.47	10.30	10.55	8.74	8.58	8.57	8.90	9.08	7.88	8.32	7.00	7.92
MnO	0.20	0.19	0.16	0.15	0.22	0.22	0.21	0.17	0.17	0.18	0.17	0.18	0.16	0.18	0.14	0.16
MgO	5.54	5.93	8.23	8.40	4.95	4.89	5.12	5.89	6.14	6.21	6.53	6.69	5.56	5.55	8.11	7.92
CaO	8.04	7.98	11.13	10.44	7.33	7.22	7.64	9.32	8.75	8.65	9.68	9.08	9.38	9.27	10.78	10.32
Na_2O	3.33	3.37	2.08	2.09	4.07	3.99	3.68	2.88	3.01	3.18	2.75	2.95	3.12	2.97	2.36	2.49
K_2O	1.57	1.53	0.28	0.09	2.67	2.55	2.21	0.21	0.09	1.34	0.28	0.99	0.07	0.07	0.30	0.20
P_2O_5	0.54	0.75	0.30	0.25	2.50	2.52	2.04	0.33	0.35	0.34	0.32	0.36	0.41	0.42	0.24	0.24
H_2O^+	3.99	2.63	3.58	4.95	1.09	1.00	2.25	2.67	2.65	2.57	3.06	3.98	3.84	3.65	2.69	3.42
Sum	100.8	100.7	101.0	100.6	101.0	100.2	99.9	99.8	99.7	100.6	100.2	100.6	99.7	99.9	100.7	101.0